Studies on the pathological mechanism of alopecia areata in C3H/HeJ mouse model

Kei Hashimoto

2022

Contents

Abbreviations

AA	alopecia areata
ASC	apoptosis-associated speck-like protein containing a caspase recruitment domain
AT	alopecia totalis
AU	alopecia universalis
CTL	cytotoxic T lymphocyte
DC	dendritic cell
H&E	hematoxylin and eosin
HF	hair follicle
HMGB1	high mobility group box-1
HSP	heat shock protein
IFN	interferon
IL	interleukin
IP	immune privilege
IRAK	interleukin-1 receptor-associated kinase
IRF	interferon regulatory factor
LN	lymph node
MHC	major histocompatibility complex
NK	natural killer
NLRP3	NOD-like receptor family pyrin domain-containing protein 3
PBMC	peripheral blood mononuclear cell
PBS	phosphate-buffered saline
pDC	plasmacytoid dendritic cell
PRR	pattern recognition receptor
RA	rheumatoid arthritis
RAGE	receptor for advanced glycation end-products
SDLN	skin-draining lymph node
SE	standard error of the mean
SLE	systemic lupus erythematosus

SSc	systemic sclerosis
Tc1	type 1 cytotoxic T
Tc2	type 2 cytotoxic T
T_{CM}	central memory T
TCR	T-cell antigen receptor
T_{EM}	effector memory T
Th1	type 1 helper T
Th2	type 2 helper T
TLR	toll-like receptor
TNF	tumor necrosis factor
TRAF	tumor necrosis factor receptor-associated factor
Treg	regulatory T
T_{RM}	resident memory T
TYRP2	tyrosinase-related protein-2

General Introduction

Alopecia areata (AA) is an autoimmune disease resulting in non-scarring hair loss with an estimated lifetime incidence to be 2.1% in the USA for 20 years (1990–2009) (1). Although the incidence rate of AA in Japan has yet been reported, Asians were reported to have a higher rate of AA than whites (2). AA may occur at any age, but 85.5% of patients developed the condition before the age of 40 years in Asian population (3). AA is not life-threatening because the manifestations of AA are confined to hair follicles (HFs) and nails. However, it significantly reduces the life quality of patients compared with atopic dermatitis or psoriasis (4, 5).

AA could be divided into clinical subtypes based on the degree of hair loss and the affected sites. The most common subtype is patchy AA, exhibiting one or multiple hair loss patches on the scalp and beard. Hair loss progresses and affects the total scalp (alopecia totalis, AT) or entire body (alopecia universalis, AU). A recent study reported that 33% of all patients suffer from patches beyond one year, which can be defined as chronic AA, and that 30% and 15% of individuals with chronic AA will ultimately develop AT and AU (6). The hair loss area and disease duration correlate with treatment non-responsiveness (7-11). Therefore, appropriate management should vary depending on the patient subtypes and disease phases. To date, an empirical treatment algorithm designed with corticosteroid and immunotherapy has been used (12-15). However, current therapies remain unsatisfactory because of numerous side effects, and a novel effective treatment based on the pathomechanism in different subtypes and disease phase is urgently needed.

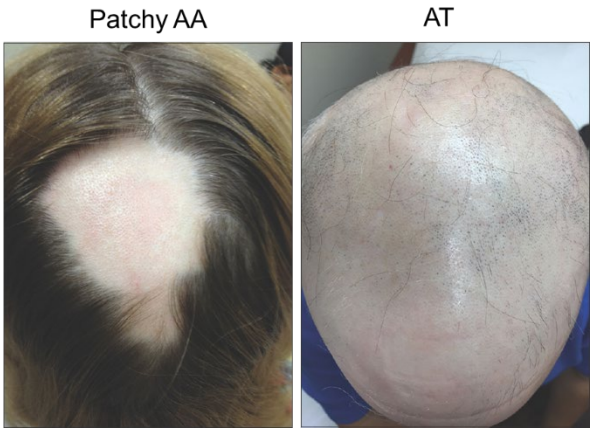

© 2018 International Journal of Trichology

Fig. G-1. Clinical manifestations of AA [16]

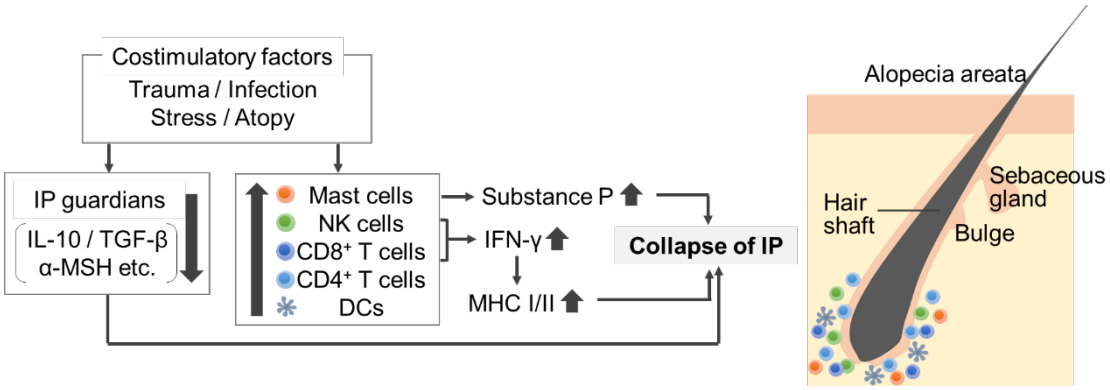

Fig. G-2. The model of AA pathogenesis

AA is thought to arise when the HF's immune privilege (IP) collapses. Natively, HFs are immune-privileged sites characterized by a number of features including the absence of lymphatic vessels, an extracellular matrix barrier, the downregulated expression of major histocompatibility complex (MHC) class I and II, and the increased production of local immunoregulatory factors such as interleukin (IL)-10, α-melanocyte-stimulating hormone and transforming growth factor β2. Thus, immunogenic autoantigens are sequestered from immune recognition in HFs. Under the genetic backgrounds, some initiators such as viral infection, vaccinations and physical stress activate both innate and adaptive immunity, which leads to IP collapses. This hypothesis is supported by

infiltration of lymphocytes, natural killer (NK) cells, dendritic cells (DCs), Langerhans cells and macrophages into the peribulbar area of anagen HFs in the acute phase. It has also been demonstrated that MHC class I and II expressions increase and IP guardians decrease in AA lesions (17-20). Genome-wide association study also implicates both adaptive immunity and innate immunity in AA pathology (21). Moreover, high-throughput T-cell antigen receptor (TCR) sequencing revealed an increase of clonality in TCRs, indicating antigen-specific T cells increase in AA patients (22). Some studies searching for autoantigens have been reported. Melanocyte and keratinocyte-derived proteins are suspected as potential autoantigens targeted by autoreactive T cells (23-26), but the exact autoantigens are still under debate. Therefore, successful identification of autoantigens is essential to elucidate the pathomechanisms and further develop the AA-specific therapeutics.

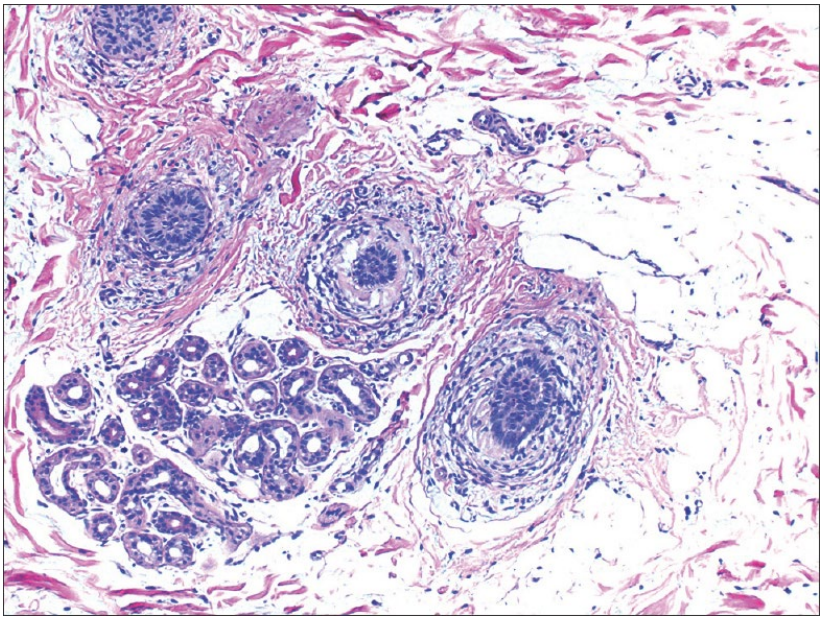

© 2018 International Journal of Trichology

Fig. G-3. Histopathology of AA patients [16]
"Swarm of bees" pattern of lymphocytes surrounding the HF

Experimental animal models could help in elucidating the disease mechanism and examining the therapeutic effects. Some rodent models have been validated and are commonly used. These include the Dundee experimental bald rat and C3H/HeJ mice (27-29). Twenty percent of female C3H/HeJ mice spontaneously develop AA-like hair loss by 18 months of age with variations in the occurrence and onset of hair loss (30). Recently, a C3H/HeJ AA mouse model was developed by grafting hair loss skin or by transferring cultured skin-draining lymph node (SDLN) cells from AA-affected mice into naïve recipients. This latter model is useful due to its high replicability and simplicity (31, 32), and it successfully responded to the immunological/pharmaceutical treatment (33, 34) in good agreement with clinical efficacy. Moreover, similar to patients with AA, its hair loss gradually progresses and spreads throughout the whole body, allowing the observation of different disease phases. However, this method requires not only spontaneous AA-affected mice but also the continuous breeding of AA mice as donor mice, which is troublesome in AA study.

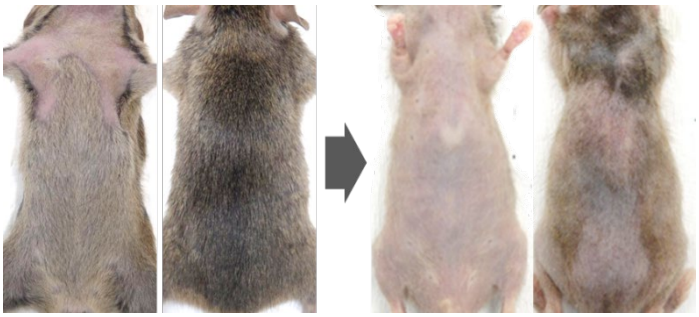

Fig. G-4. C3H/HeJ mouse model of AA
Hair loss starts at the ventral axillary region and spreads to the dorsal skin.

In this study, the author aimed at elucidating the underlying mechanisms of AA using the mouse model, expecting that the findings of this study could lead to develop a novel AA therapeutics. In chapter 1, to elucidate the pathological differences between the acute and chronic AA phases, the author analyzed local or systemic T cell subpopulations, cytokines, chemokines and antigen presentation-related molecule expressions of the acute and chronic-AA mice. Further, to identify common autoantigens of patients with AA, the serum levels of autoantigen antibodies were determined and the autoantigen-specific T

cells in SDLNs were directly detected. The results indicated that T cell subpopulations contributing to the pathogenesis of AA are different between the disease phases and tyrosinase is one of autoreactive targets in the AA mouse model as well as in patients with AA. In chapter 2, to solve the troublesome matter in generating the AA mouse model, the author established a new method for generating the model using cryopreserved lymphocytes with a high incidence. This convenient and reproducible method is expected to be valuable for AA study. Last, to clarify the contribution of innate immune system to initiation of AA, the change of NOD-like receptor family pyrin domain-containing protein 3 (NLRP3) inflammasome activation, comparing before and after AA onset, and the therapeutic effect of NLRP3 inflammasome inhibitor were investigated in chapter 3. The findings revealed that inhibition of NLRP3 inflammasome may be a promising therapeutic approach to AA.

Chapter 1

Altered T cell subpopulations during the disease phases of alopecia areata and analysis of candidate autoantigens in the C3H/HeJ mouse model*

*The content described in Chapter 1 was originally published in *Journal of Dermatological Science*. Hashimoto K, Yamada Y, Fujikawa M, Sekiguchi K, Uratsuji H, Mori S, Watanabe H, Matsumoto T. Altered T cell subpopulations and serum anti-TYRP2 and tyrosinase antibodies in the acute and chronic phase of alopecia areata in the C3H/HeJ mouse model. *J. Dermatol. Sci*. 2021;**104**(1):21-29.

1.1 Introduction

AA could be divided into four clinical subtypes, based on the degree of hair loss and affected sites. The pathological features vary by disease factors (hair loss area, disease duration, disease activity, etc.), and which correlate with treatment non-responsiveness (7-11, 35). Revealing the differences of pathology between various disease phases would be valuable to choose the appropriate management, but the pathological differences are still unknown.

HFs are immune-privileged sites, in which immunogenic autoantigens are sequestered from immune recognition (36). The collapse of IP is suggested to cause AA development (17, 18). Melanin-generating anagen HFs targeted by immune response, as indicated by the regrowth of gray hair in AA lesions, and melanogenesis-related proteins have been suggested as autoantigens in AA. Tyrosinase and tyrosinase-related protein-2 (TYRP2, dopachrome tautomerase), which are highly conserved melanogenic enzyme, induced $CD8^+$ T cell activation in the peripheral blood mononuclear cells (PBMCs) of patients with AA, correlating with the AA extent and duration (23). Melanoma associated antigen 3-specific T cells increased in the PBMCs of patients with AA compared to that of the healthy controls (26). Therefore, the identification of the exact autoantigens is still under debate and the autoantigens seem to vary across the patients with AA.

Experimental animal models could help in elucidating the disease mechanism and examining the therapeutic effects. The C3H/HeJ AA mouse model developed by transferring cultured SDLN cells from AA-affected mice is useful due to its high replicability (31, 32) and its high similarity with clinical efficacy. Moreover, similar to patients with AA, its hair loss gradually progresses and spreads throughout the whole body, allowing the observation of different disease phases. Therefore, to better understand the underlying mechanisms of AA in each phase and estimate the clinical efficacy of AA therapeutic agents, it would be potentially interesting to elucidate the pathological differences between the acute and chronic-AA phases in this model.

In this chapter, we analyzed T cell subpopulations in PBMCs, SDLN cells, and infiltrating cells into the skin of the AA mouse model, not only by comparing the non-lesions with the lesions of AA mice but also by comparing acute with chronic-AA. We

also determined the cytokine, chemokine, and antigen presentation-related molecule expression in the serum and skin of acute and chronic-AA mice. Finally, to identify common autoantigens with patients with AA, the serum levels of autoantigen antibodies were determined, and the autoantigen-specific T cells in the SDLNs were directly detected.

1.2 Materials and Methods

1.2.1. AA mouse model

Female 7-week-old C3H/HeJ mice obtained from Japan SLC (Shizuoka, Japan) received food pellet for long-term breeding (CR-LPF; Oriental Yeast, Tokyo, Japan) and ultraviolet-sterilized water *ad libitum* under specific-pathogen-free conditions. All animal experiments were performed in accordance with the "Guiding Principles for the Care and Use of Animals in the Field of Physiological Sciences" of the Physiological Society of Japan. All animal experimental procedures were approved by the Ethics Committee for Animal Experiments of Maruho (Kyoto, Japan) and were conducted in accordance with the "Guiding Principles for the Care and Use of Laboratory Animals" at Maruho.

AA mice were induced by transferring *in vitro* expanded lymph node (LN) cells from AA-affected mice as described previously (31, 32) with minor modifications. Briefly, SDLN cells (cervical, axillary, inguinal, and popliteal LN) were obtained from previously AA-affected mice (induced by transferring expanded LN cells, with S4 hair loss score) and prepared in RPMI-1640 (Thermo Fisher Scientific, Waltham, MA, USA) supplemented with 10% fetal bovine serum (MP Biomedicals, Santa Ana, CA, USA), 100 U/mL penicillin-streptomycin (Nacalai Tesque, Kyoto, Japan), 2 mM GlutaMAX (Thermo Fisher Scientific), 30 U/mL recombinant human IL-2 (Roche Diagnostics GmbH, Mannheim, Germany), 25 ng/mL recombinant mouse IL-7 (R&D Systems, Minneapolis, MN, USA) and 50 ng/mL recombinant mouse IL-15 (R&D Systems). Cells were activated with Dynabeads Mouse T-Activator CD3/CD28 (Thermo Fisher Scientific) and cultured for 7 days. Twenty million cells were injected intradermally to a naïve 8-week-old C3H/HeJ mouse. Mice were divided into the following groups: naïve

mice, without transferring LN cells; unaffected mice, transferred LN cells without hair loss; acute-AA mice, with hair loss in the abdominal area for less than 2 weeks; chronic-AA mice, with hair loss in the whole abdominal and part of the dorsal area for more than 4 weeks.

1.2.2. Cell preparation

SDLNs were minced and filtered to prepare single-cell suspensions. The PBMCs were isolated from the blood using Ficoll-Paque PREMIUM (Cytiva, Tokyo, Japan). Punch biopsies were taken from the non-lesions (hairy area), boundaries with half non-lesions and half lesions, and lesions (hairless area), and incubated in 1 mg/mL collagenase type I (FUJIFILM Wako Pure Chemical, Osaka, Japan) for 30 min at 32°C.

1.2.3. Flow cytometric analysis

To prepare single-cell suspensions, cell samples were filtered through a 70-μm cell strainer (Falcon, NY, USA). The single-cell suspensions were pre-incubated with anti-CD16/32 (Thermo Fisher Scientific) in MACS Buffer (autoMACS Rinsing Solution containing 0.5% bovine serum albumin; Miltenyi Biotec, Bergisch Gladbach, Germany) to block nonspecific binding of antibodies to FcγR. The cells were incubated with fluorochrome-conjugated antibodies and stained with 7-AAD (eBioscience, San Diego, CA, USA) or a LIVE/DEAD Fixable Aqua Dead Cell Stain Kit (Thermo Fisher Scientific) to exclude non-viable cells. The flow cytometric analysis was conducted using FACSAriaIII and FlowJo analysis software (BD Biosciences, San Jose, CA, USA). The fluorochrome-conjugated antibodies were as follows: CD3 and CD8 (145-2C11 and 53-6.7, respectively, BD Biosciences); CD4 (GK1.5, BioLegend, CA, USA); NKG2D, CXCR3, CD44, and CD62L (CX5, CXCR3-173, IM7, and MEL-14, respectively, eBioscience). The cell population was identified as follows: effector memory T cell/resident memory T cell (T_{EM}/T_{RM}; $CD44^+CD62L^-$), central memory T cell (T_{CM}; $CD44^+CD62L^+$), type 1 helper T cell (Th1; $CD4^+CXCR3^+$), and type 1 cytotoxic T cell (Tc1; $CD8^+CXCR3^+$).

The tyrosinase- and TYRP2-specific $CD8^+$ cells were detected using the QuickSwitch Quant H-$2K^b$ Tetramer Kit-PE (MBL, Aichi, Japan). The H-$2K^b$ Negative Tetramer SIYRYYGL (MBL) was used as a control. The tyrosinase peptide (KNKFFSYL) and TYRP2 peptide (SVYDFFVWL) were used to generate peptide-specific tetramers according to the manufacturer's instructions.

1.2.4. Quantitative real-time PCR

To determine mRNA expressions, total RNA was isolated from homogenized skin samples using an RNeasy Fibrous Tissue Mini Kit (Thermo Fisher Scientific). cDNA was synthesized by the reverse transcription of total RNA using a High Capacity cDNA Reverse Transcription Kit, amplifying with the TaqMan Gene Expression Master Mix and TaqMan Gene Expression Assay (Thermo Fisher Scientific). The primer sets purchased from Thermo Fisher Scientific were as follows: *B2m* (Mm00437762_m1), *Ccl9* (Mm00839966_g1), *Cxcl9* (Mm00434946_m1), *Cxcl10* (Mm00445235_m1), *Cxcl11* (Mm00444662_m1), *Gzmb* (Mm00442837_m1), *H2-Ab1* (Mm00439216_m1), *Ifng* (Mm01168134_m1), *Il12b* (Mm01288989_m1), *Prf1* (Mm00812512_m1), *Tyr* (Mm00495817_m1), *Tyrp2* (Mm01225584_m1), and *Gapdh* (Mm99999915_g1). The results were normalized to *Gapdh* and analyzed with QuantStudio 7 Flex Real-Time PCR System and StepOnePlus System (Thermo Fisher Scientific).

1.2.5. Multiplex assay

The interferon (IFN)-γ concentration in the serum was measured by the Bio-Plex Multiplex Immunoassay System using a Bio-Plex Pro Mouse Cytokine Th1/ type 2 helper T cell (Th2) Assay (Bio-Rad, Hercules, CA, USA).

1.2.6. Immunohistochemical staining

Frozen skin sections were fixed in methanol/acetone (1:1) or acetone (–20°C) and stained with primary antibodies: anti-CD11c (N418, Thermo Fisher Scientific) and anti-MHC Class I (ER-MP42, BMA Biomedicals, Augst, Switzerland). Alexa Fluor 488-

conjugated anti-Hamster IgG(H + L) and Alexa Fluor 568-conjugated anti-Rat IgG(H + L) (Thermo Fisher Scientific) were used as secondary antibodies. Hoechst 33,342 (Thermo Fisher Scientific) was used for nuclear staining. Images were obtained by a confocal laser scanning microscope (Olympus, Tokyo, Japan).

1.2.7. Enzyme-linked immunosorbent assay (ELISA)

Blood samples were collected under anesthesia and serum was isolated after coagulation and centrifugation. The serum autoantibody concentration was measured by ELISA, using 0.03 mg/mL of tyrosinase protein (CUSABIO, Wuhan, China) and 0.1 mg/mL of TYRP2 protein (Abcam, Cambridge, UK) as coating antigens for the anti-tyrosinase and anti-TYRP2 antibodies, respectively, and horseradish peroxidase-conjugated goat anti-mouse IgG antibody (Thermo Fisher Scientific) as a detection antibody. The concentrations were divided by the total IgG.

1.2.8. Statistical analysis

Data are expressed as the mean ± standard error of the mean (SE). The statistical analysis was conducted using Dunnett's multiple comparison test, as implemented in EXSUS (CAC Croit, Tokyo, Japan). *P*-values less than 0.05 were considered statistically significant.

1.3 Results

1.3.1. Increased $CD8^+NKG2D^+$ T and T_{EM} cell percentages among the SDLN cells depending on AA chronicity and those among the PBMCs in the unaffected and acute-AA mice

As previously reported (32), hair loss began at the abdominal side with subsequent dorsal expansion in this AA model. To clarify the relationship between the hair loss and the lymphocyte population alterations, we first investigated the number of SDLN cells in naïve, unaffected, and AA mice at different disease stages. In the acute-AA mice, hair loss

was localized at the periphery of the axillary and inguinal region at the abdominal side and the numbers of axillary and inguinal LN cells increased compared with those of naïve and unaffected mice (Fig. 1-1A). In chronic-AA mice, the hair loss spread to the dorsal side and the head. Concomitantly, the numbers of the axillary and cervical LN cells increased compared with those of the acute phase (Fig. 1-1A). These results correspond to regional SDLN restrictions (head and neck drained by cervical LNs, upper extremity and trunk by axillary LNs, the lower extremity by inguinal LNs, and the hind paws by popliteal LNs) (37).

Next, we further investigated the $CD8^+$ T cell subpopulations in AA mice through flow cytometric analysis of the SDLN cells and PBMCs. The percentages of Tc1 cells among the cervical and axillary LN cells increased only for chronic-AA, and those among the PBMCs increased depending on AA chronicity (Fig. 1-1B). The serum IFN-γ level increased in AA mice, especially in chronic-AA mice (Fig. 1-1C). The $CD8^+NKG2D^+$ T and $CD8^+$ T_{EM} cell percentages among the SDLN cells increased depending on AA chronicity. The $CD8^+NKG2D^+$ T and $CD8^+$ T_{EM} cell percentages among the PBMCs were the highest in the unaffected and acute-AA mice, respectively (Fig. 1-1D, E). The $CD8^+$ T_{CM} cell percentages among the cervical and inguinal LN cells and PBMCs increased in the AA mice depending on AA chronicity (Fig. 1-1F).

Fig. 1-1. The $CD8^+NKG2D^+$ T and T_{EM} cell percentages increased in the SDLN depending on AA chronicity and those of PBMCs in the unaffected mice and acute-AA mice.

(A) Cell counts of cervical, axillary, inguinal, and popliteal LN cells from naïve, unaffected, and AA-affected mice. The percentages of (B) Tc1 cells, (D) $CD8^+NKG2D^+$ T cells, (E) $CD8^+$ T_{EM} cells, and (F) $CD8^+$ T_{CM} cells to $CD3^+$ T cells in the LN cells and PBMCs assessed by flow cytometric analysis. (C) Serum IFN-γ levels measured by multiplex assay. Data are expressed as the mean ± SE (N = 3–4). ‡$p < 0.05$. ‡‡$p < 0.01$. vs. naïve mice (Dunnett's multiple comparison test). N, naïve mice; U, unaffected mice; A, acute-AA mice; C, chronic-AA mice.

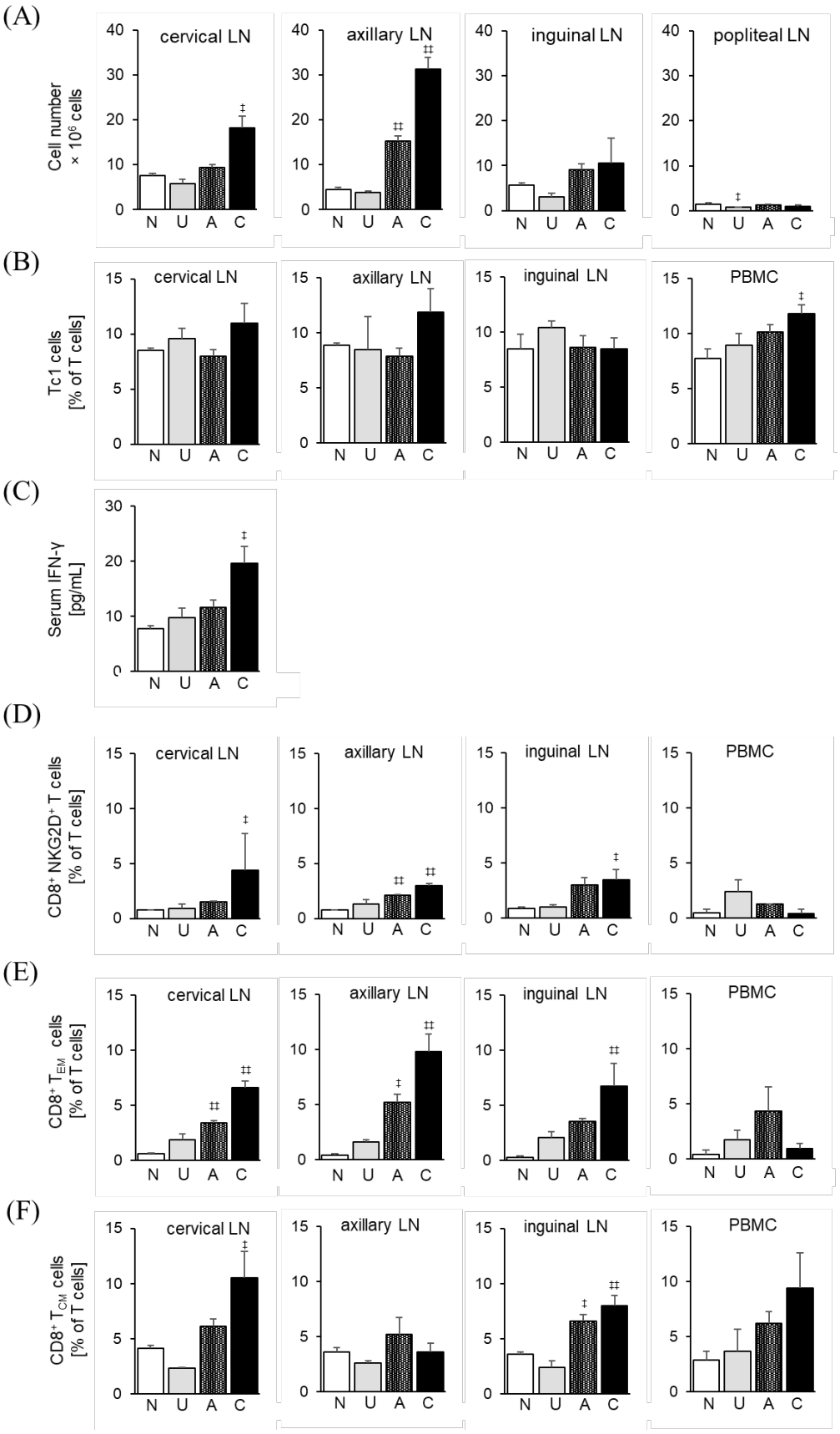
(A)
Cell number × 10^6 cells
cervical LN
axillary LN
inguinal LN
popliteal LN
(B)
Tc1 cells [% of T cells]
cervical LN
axillary LN
inguinal LN
PBMC
(C)
Serum IFN-γ [pg/mL]
(D)
CD8+ NKG2D+ T cells [% of T cells]
cervical LN
axillary LN
inguinal LN
PBMC
(E)
CD8+ TEM cells [% of T cells]
cervical LN
axillary LN
inguinal LN
PBMC
(F)
CD8+ TCM cells [% of T cells]
cervical LN
axillary LN
inguinal LN
PBMC
N U A C

1.3.2. Increased Th1 and $CD4^+$ T_{EM} cell percentages among the SDLN cells and PBMCs in the unaffected and AA-affected mice

As the $CD4^+$ and $CD8^+$ T cells were suggested to participate in AA pathology, the $CD4^+$ T cell subpopulations among the SDLN cells and PBMCs in AA mice were analyzed using flow cytometry. The Th1 ($CD4^+CXCR3^+$) cell percentages among the SDLN cells and PBMCs increased in the unaffected mice compared with the naïve mice and the acute-AA mice, and those in the chronic-AA mice were higher than those in the acute-AA mice (Fig. 1-2A). The $CD4^+$ T_{EM} cell percentages among the SDLN cells and PBMCs were higher in the unaffected and AA mice compared with the naïve mice (Fig. 1-2B), whereas those of the $CD4^+$ T_{CM} cells among the SDLN cells remained unchanged or decreased in the unaffected and AA mice compared with those in the naïve mice. The $CD4^+$ T_{CM} cell percentage among the PBMCs increased depending on the AA chronicity (Fig. 1-2C).

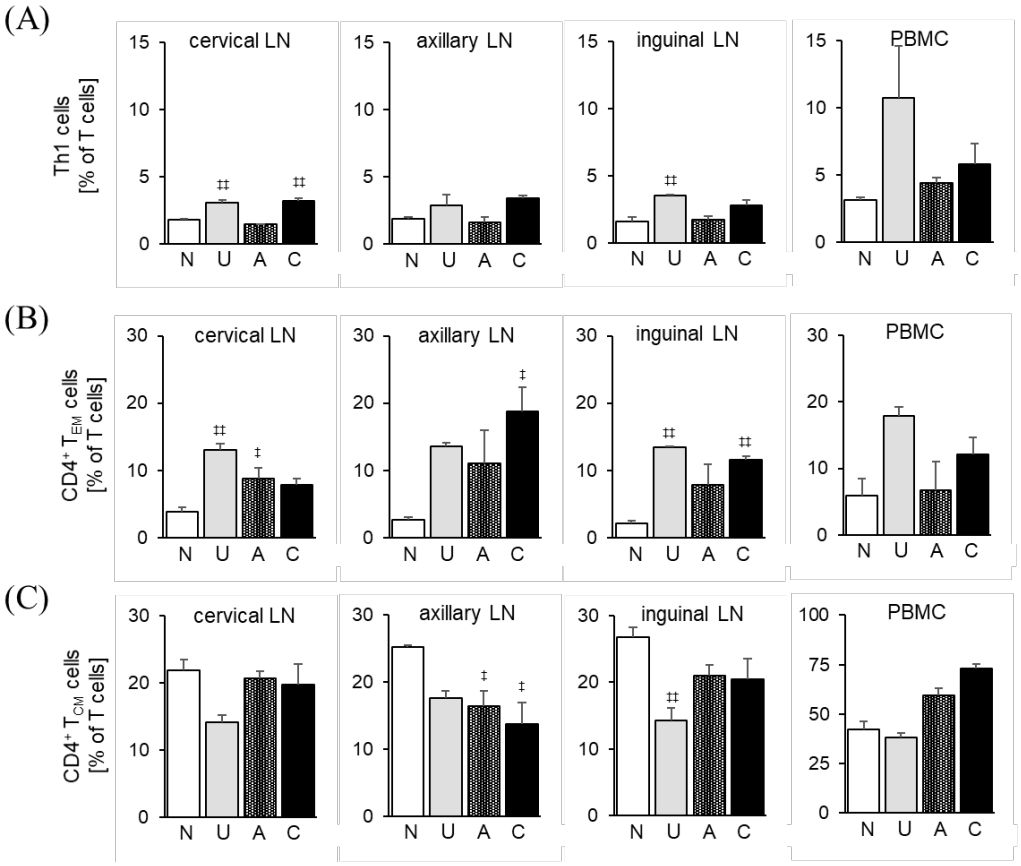

Fig. 1-2. The Th1 and CD4$^+$ T_{EM} cells among the SDLN cells and PBMCs increased in unaffected and AA mice.

Percentages of (A) Th1, (B) CD4$^+$ T_{EM} cells, and (C) CD4$^+$ T_{CM} cells compared to CD3$^+$ T cells among the LN cells and PBMCs assessed by flow cytometric analysis. Data are expressed as the mean ± SE (N = 3). ‡$p < 0.05$. ‡‡$p < 0.01$. vs. naïve mice (Dunnett's multiple comparison test). N, naïve mice; U, unaffected mice; A, acute-AA mice; C, chronic-AA mice.

(A)

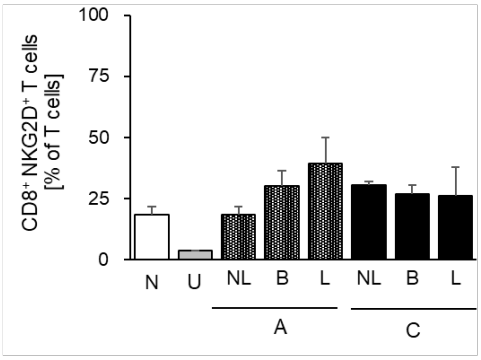
CD8+ NKG2D+ T cells
[% of T cells]
100
75
50
25
0
N
U
NL
B
L
NL
B
L
A
C

(B)

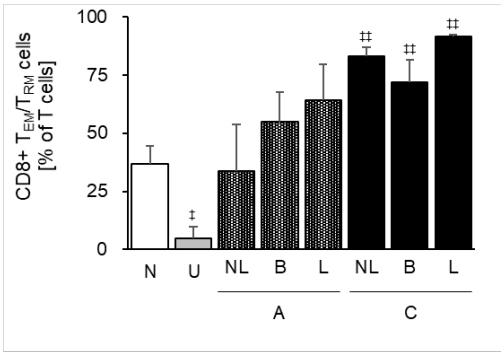
CD8+ TEM/TRM cells
[% of T cells]
100
75
50
25
0
‡
‡‡
‡‡
‡‡
N
U
NL
B
L
NL
B
L
A
C

(C)

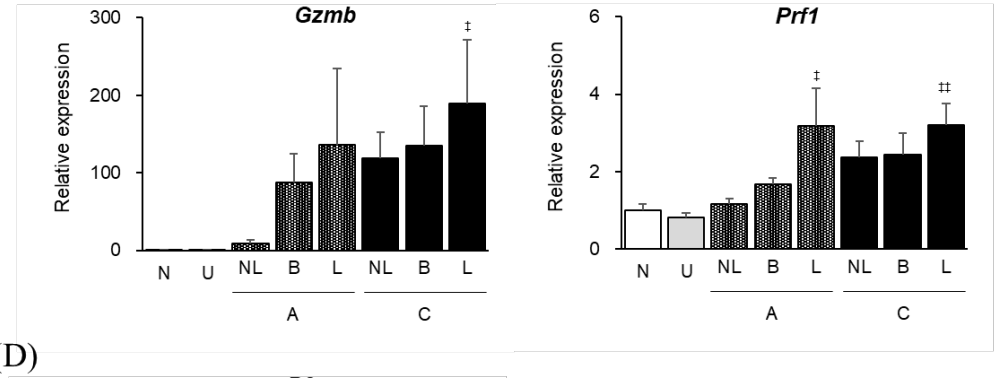
Gzmb
Relative expression
300
200
100
0
‡
N
U
NL
B
L
NL
B
L
A
C
Prf1
Relative expression
6
4
2
0
‡
‡‡
N
U
NL
B
L
NL
B
L
A
C

(D)

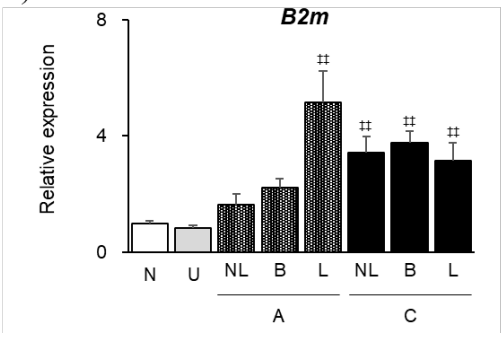
B2m
Relative expression
8
4
0
‡‡
‡‡
‡‡
N
U
NL
B
L
NL
B
L
A
C

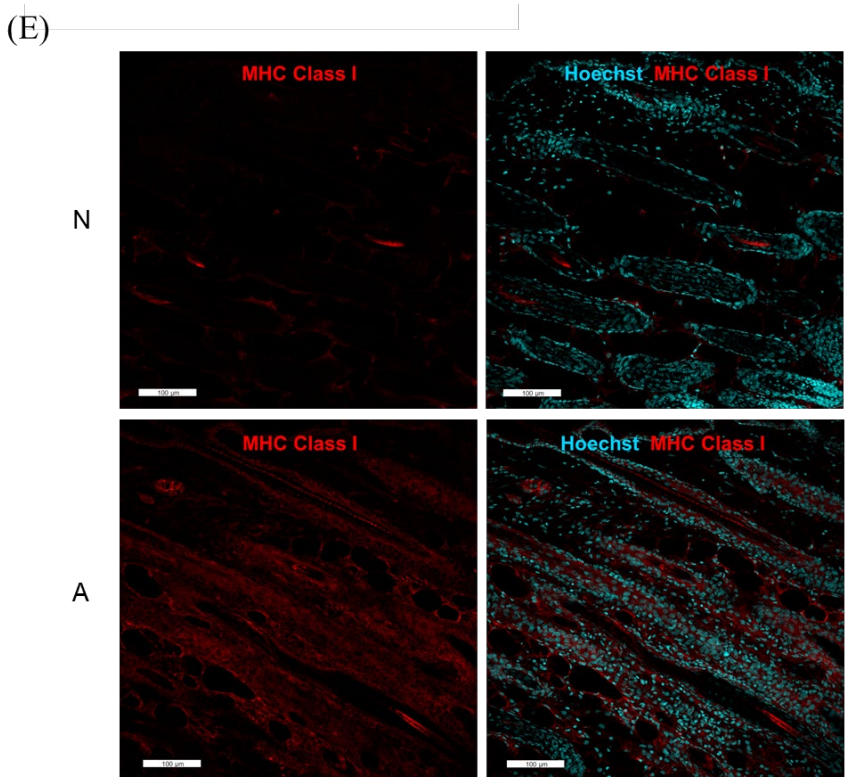

Fig. 1-3. The CD8$^+$ T cell populations and MHC class I expression increased in the skin of acute- and chronic-AA mice.

Percentages of (A) CD8$^+$NKG2D$^+$ T cells and (B) CD8$^+$ T_{EM}/T_{RM} cells compared to CD3$^+$ T cells in the skin assessed by flow cytometric analysis. (C, D) mRNA (*Gzmb*, *Prf1*, and *B2m*) expressions in the skin analyzed by RT-qPCR. (E) Immunohistochemical staining of MHC class I in the skin from a naïve mouse and acute-AA mouse. Data are expressed as the mean ± SE (N = 3-5). ‡$p < 0.05$. ‡‡$p < 0.01$. vs. naïve mice (Dunnett's multiple comparison test). N, naïve mice; U, unaffected mice; A, acute-AA mice; C, chronic-AA mice. NL, non-lesion; B, lesion boundary; L, lesion.

1.3.3. Increased $CD8^+$ T cell populations and MHC class I expression in both the acute- and chronic-AA mice skin

Next, we investigated the infiltrating $CD8^+$ T cell populations and the expression of related proteins in the non-lesions, boundaries, and lesions. The $CD8^+NKG2D^+$ T and $CD8^+$ T_{EM}/T_{RM} cell percentages were upregulated in the lesions of the acute-AA mice and the non-lesions, boundaries, and lesions of chronic-AA mice (Fig. 1-3A, B). In the acute-AA mice, the granzyme B and perforin 1 mRNA expression levels, corresponding to enzymes expressed in cytoplasmic granules of cytotoxic T lymphocytes (CTLs) and NK cells, in the non-lesions were almost equal to those of the naïve and unaffected mice, and elevated in the lesions of the acute-AA mice and the non-lesions, boundaries, and lesions of the chronic-AA mice (Fig. 1-3C). These observations indicated that, similar to clinical AA, the $CD8^+NKG2D^+$ T cells and $CD8^+$ T_{EM}/T_{RM} cells accumulate in the skin of this AA model, suggesting an ectopically-induced MHC class I antigen presentation. Furthermore, we measured the β2-microglobulin mRNA expression, corresponding to a component of MHC class I molecules, in the skin. In the acute- and chronic-AA mice, the *B2m* level was higher than in the naïve and unaffected mice, and it significantly increased in the lesions (Fig. 1-3D). MHC class I^+ cells were increased in the skin of acute-AA mice compared with naïve mice. (Fig. 1-3E)

1.3.4. Increased level of Th1 cell percentages, DC-related cytokines, and MHC class II expression in the AA mice skin

We also investigated the infiltrating $CD4^+$ T cell populations in the skin. Although the Th1 cell percentages in the skin were lower than those of the $CD8^+$ T cell populations, the Th1 cell cutaneous infiltration in AA mice increased compared with that in the naïve and unaffected mice (Fig. 1-4A). Concomitantly, the IFN-γ mRNA level increased in AA mice (Fig. 1-4B). Moreover, the Th1/Tc1 chemokine, such as CXCL9, CXCL10, and CXCL11, mRNA levels increased depending on the hair loss symptoms in both acute-AA and chronic-AA mice (in the boundaries, lesions, and also the non-lesions of the latter) (Fig. 1-4C).

Furthermore, to investigate the Th1-polarizing DC involvement, we measured the DC-related chemokine and cytokine expression. The CCL19 mRNA level, attracting DCs by binding to the receptor CCR7, was elevated in the AA mice boundaries and lesions (Fig. 1-4D). The IL-12β mRNA level, produced by mature DCs, was elevated in the acute-AA mice lesions and chronic-AA mice boundaries and lesions (Fig. 1-4D). Similar to these cytokines, the MHC class II (*H2-Ab1*) mRNA level also increased in AA-affected mice (Fig. 1-4E). $CD11c^+$ cells were infiltrated around HFs in the acute-AA mice (Fig. 1-4F).

1.3.5. Highly-upregulated anti-tyrosinase antibody serum levels and tyrosinase-specific $CD8^+$ T cells in AA mice

The hair matrix keratinocyte and melanocyte antigens were suggested as potential autoreactive cytotoxic T cell targets, important for AA onset and progression (23, 38). Therefore, we next focused on melanogenesis-related molecules (TYRP2, tyrosinase) as convincing candidate autoantigens, and detected their mRNA expressions in the AA mice skin. The mRNA levels of both molecules in the AA mice lesions decreased compared with those in the naïve and unaffected mice, just as well as the AA mice non-lesions (Fig. 1-5A). Nevertheless, the anti-TYRP2 antibody serum levels slightly increased in the unaffected and AA-affected mice compared with those in the naïve mice, and the anti-tyrosinase antibody serum levels were higher in the unaffected and AA mice than those in the naïve mice (Fig. 1-5B). Furthermore, our flow cytometric analysis using MHC class I tetramer revealed that the TYRP2- and especially the tyrosinase-specific $CD8^+$ T cells were upregulated in the unaffected and AA mice (Fig. 1-5C).

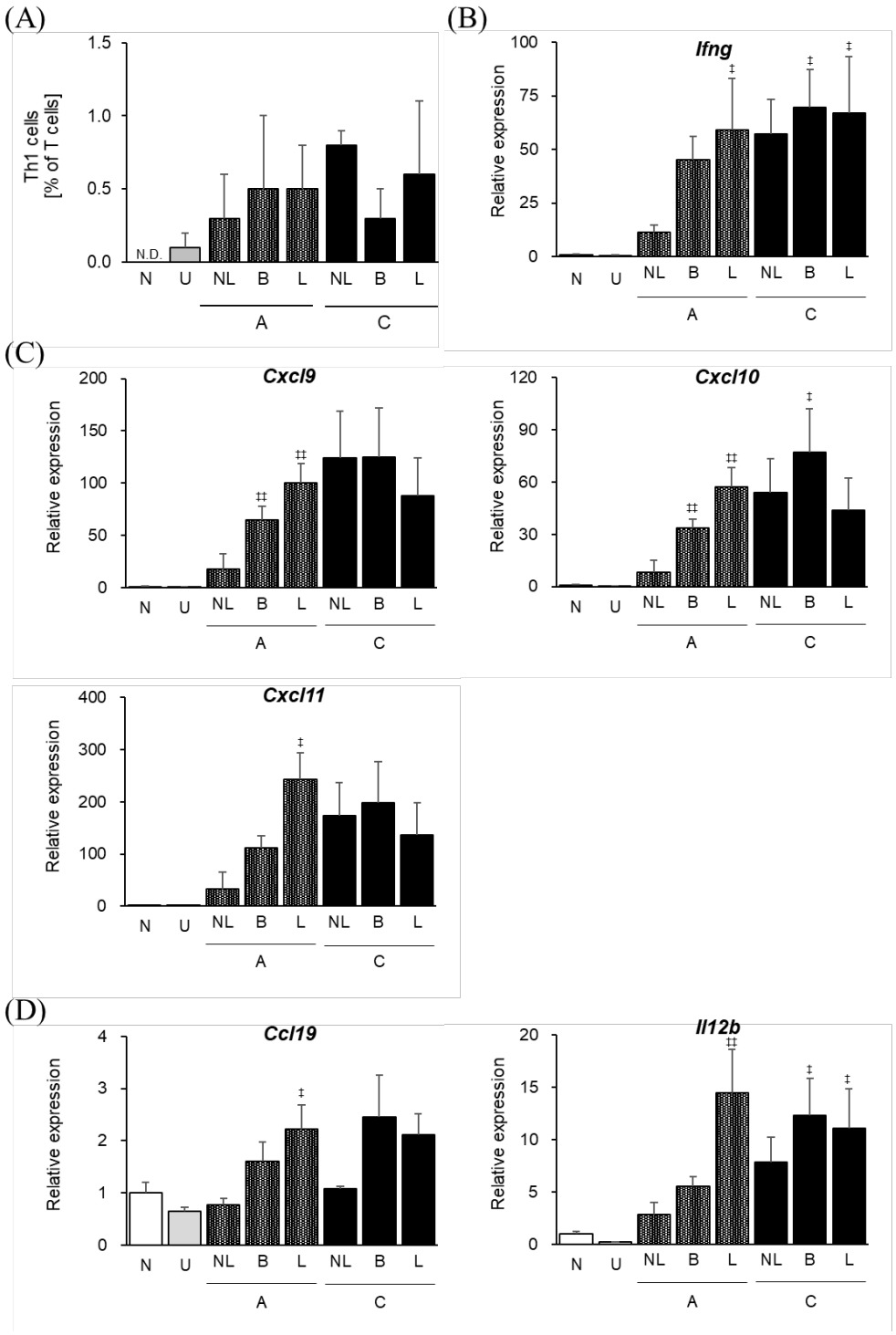
(A)
Th1 cells
[% of T cells]
1.5
1.0
0.5
0.0
N.D.
N U NL B L NL B L
A C
(B)
Ifng
Relative expression
100
75
50
25
0
‡
N U NL B L NL B L
A C
(C)
Cxcl9
Relative expression
200
150
100
50
0
‡‡
‡
N U NL B L NL B L
A C
Cxcl10
Relative expression
120
90
60
30
0
‡‡
‡
N U NL B L NL B L
A C
Cxcl11
Relative expression
400
300
200
100
0
‡
N U NL B L NL B L
A C
(D)
Ccl19
Relative expression
4
3
2
1
0
‡
N U NL B L NL B L
A C
Il12b
Relative expression
20
15
10
5
0
‡‡
‡
‡
N U NL B L NL B L
A C

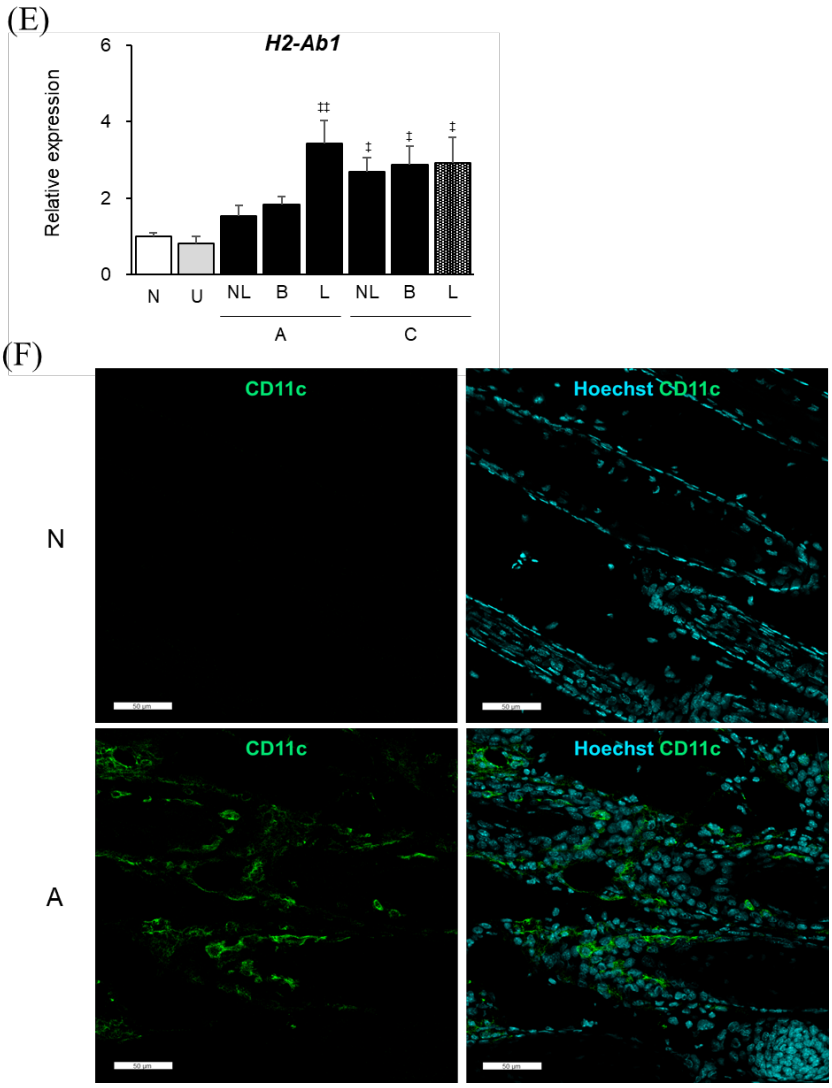

Fig. 1-4. The Th1 cells, DC-related cytokines, and MHC class II expression increased in the skin of acute- and chronic-AA mice.

(A) Percentage of Th1 cells compared to $CD3^+$ T cells in the skin assessed by flow cytometric analysis. (B-E) mRNA (*Ifng*, *Cxcl9*, *Cxcl10*, *Cxcl11*, *Ccl19*, *Il12b*, and *H2-Ab1*) expressions in the skin analyzed by RT-qPCR. (F) Immunohistochemical staining of CD11c in the skin from a naïve mouse and acute-AA mouse. Data are expressed as the mean ± SE (N = 3-5). ‡$p < 0.05$. ‡‡$p < 0.01$. vs. naïve mice (Dunnett's multiple comparison test). N, naïve mice; U, unaffected mice; A, acute-AA mice; C, chronic-AA mice. NL, non-lesion; B, lesion boundary; L, lesion. N.D., not detected.

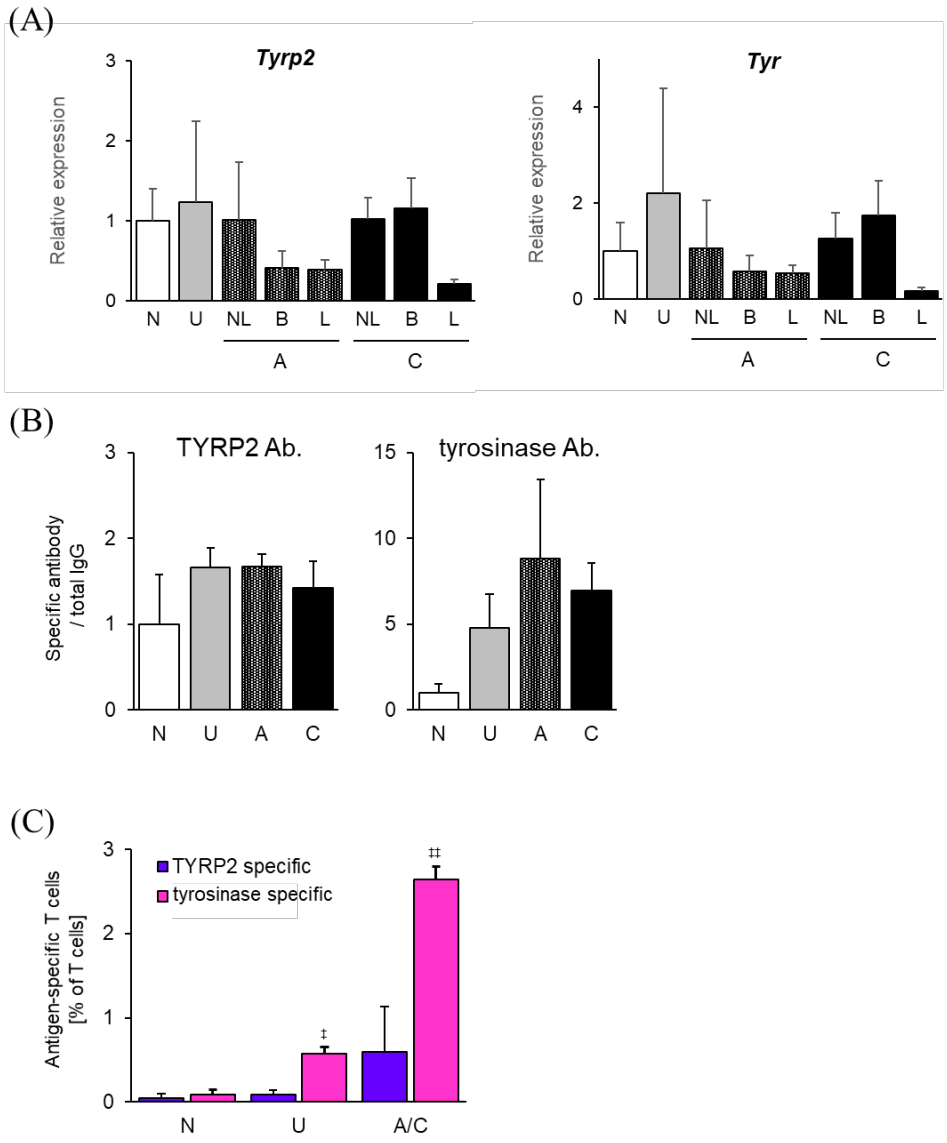

Fig. 1-5. The TYRP2 and tyrosinase-specific CD8$^+$ T cells and serum anti-TYRP2 and tyrosinase antibodies were upregulated in AA mice.

(A) mRNA (*Tyrp2* and *Tyr*) expressions in the skin analyzed by RT-qPCR. (B) Serum anti-TYRP2 and anti-tyrosinase antibodies measured by ELISA. (C) TYRP2- and tyrosinase-specific CD8$^+$ T cells among the LN cells detected by flow cytometric analysis. Data are expressed as the mean ± SE (N = 3-4). ‡$p < 0.05$. ‡‡$p < 0.01$. vs. naïve mice (Dunnett's multiple comparison test). N, naïve mice; U, unaffected mice; A, acute-AA mice; C, chronic-AA mice; A/C, acute- and chronic-AA mice. NL, non-lesion; B, lesion boundary; L, lesion. TYRP2, tyrosinase-related protein-2.

1.4 Discussion

It was demonstrated that the $CD8^+$ and $CD4^+$ T cell subpopulation percentages and cytokine and chemokine expression levels differ between the disease phases, and the MHC class I and II expressions increase in the AA mice skin. Moreover, TYRP2 and tyrosinase were identified as autoantigen targets in the AA mice.

CTLs reportedly contribute to AA development (18, 39, 40). We found that the Tc1 cell percentages among the PBMCs and the serum IFN-γ levels were higher in the chronic than in the acute phase (Fig. 1-1B and C). The cytotoxic mediator granzyme B and perforin 1 mRNA expression levels increased not only in the acute- and chronic-AA mice lesions but also in the chronic-AA mice non-lesions (Fig. 1-3C). These alterations between the phases correlated with the clinical observations that the Tc1 cell percentages among PBMCs were higher in the chronic phase and that Tc1 cells infiltrated HFs in both the acute and chronic phase (41), finally, that the serum IFN-γ levels correlated with AA activity and disease duration (42). These data suggest a systemically-enhanced cytotoxic activity but also a CTL localization in the lesions in acute-AA mice, and in the non-lesions as well as the lesions in chronic-AA mice. The $CD8^+NKG2D^+$ T and $CD8^+$ T_{EM}/T_{RM} cell percentages in the LNs and skin also increased in the chronic phase (Fig. 1-1D, E, Fig. 1-3A, B), indicating that they contribute to HF attacking and lasting hair loss, in accordance with previous reports in patients with AA and other AA mouse models (34, 40, 43). In contrast, the percentage of these populations in the PBMCs increased in the unaffected and acute-AA, but not in the chronic-AA mice (Fig. 1-1D, E). Conversely, the $CD8^+$ T_{CM} cell percentages among the PBMCs increased in the chronic phase compared to those in the acute phase (Fig. 1-1F). The $CD8^+NKG2D^+$ T and $CD8^+$ T_{EM} cells might thus migrate into the skin, reside there, and the $CD8^+$ T_{CM} cells remain in circulation with their different trafficking properties (44, 45). However, the underlying mechanisms remain unclear.

Not only $CD8^+$ but also $CD4^+$ T cells reportedly participate in AA pathology (40, 46). The Th1 and $CD4^+$ T_{EM} cell percentages in the LNs increased in both the unaffected and AA mice (Fig. 1-2A, B), indicating that the $CD4^+$ T cell increase occurred in an earlier phase than that of the $CD8^+$ T cells. The increase rate of $CD4^+$ T_{EM} cells was higher than that of $CD8^+$ T_{EM} cells (Fig. 1-1E, 2B). The preceding change in $CD4^+$ T cell percentage

in this model is similar to the clinical observation that the immunological state of the circulating T cells is suggested to be polarized to the Th1 cells in the acute phase in patients with AA (41). The results suggest that $CD4^+$ T cell priming and DC-mediated antigen-specific activation occur in the LNs before and after the AA onset. The $CD4^+$ T_{CM} cells were dominant in the LNs and among the PBMCs, the former decreasing and the latter increasing in AA mice (Fig. 1-2C). We speculate that the systemic $CD4^+$ T_{CM} cells differentiated into $CD4^+$ T_{EM} cells in the lymphatic circulation. Although the systemic Th1 cell percentages were lower in the acute-AA mice than in the unaffected mice (Fig. 1-2A), the cutaneous Th1 cell infiltration increased in the AA-affected mice (Fig. 1-4A), suggesting that local infiltration and accumulation of Th1 cells induce AA onset. The IFN-γ mRNA expression and Th1-type chemokine mRNA expressions also increased depending on the acute-AA mice hair loss symptoms and in the chronic-AA mice non-lesions, boundaries, and lesions (Fig. 1-4B, C), in accordance with the clinical pathology (41, 47). We also found that the CCL19 mRNA level was upregulated in the AA mice boundaries and lesions, and the *Il12b* expression, encoding the common IL-12p40 subunit of IL-12 and IL-23, increased in the acute-AA mice lesions, just as well as the chronic-AA mice boundaries and lesions (Fig. 1-4D). DC-derived CCL19 is a reported chemo-attractant of $CCR7^+$ T cells and DCs, modulating T cell survival and trafficking (48). Macrophage- or DC-derived IL-12 activates NK cells and CTLs, and DC-derived IL-23 promotes IL-17 secretion in T cells (49, 50). Furthermore, we found that the MHC class II expression levels increased and $CD11c^+$ cells infiltrated around the HFs in the AA mice skin (Fig. 1-4E, F). These data suggest that DCs infiltrate the skin and locally present antigens to T cells like psoriasis (51) besides the cutaneous infiltration of the LN-educated T cells. Taken together, the following factors in the chronic-AA mice non-lesions increased to the level of factors in the acute- and chronic-AA mice lesions: $CD8^+NKG2D^+$ T and $CD8^+$ T_{EM}/T_{CM} cells, granzyme B, perforin 1, MHC class I/II, and Th1/Tc1 chemokines. The DC-related chemokine CCL9 and cytokine IL-12β expression levels were higher in the chronic-AA mice lesions compared with those in the acute- and chronic-AA mice non-lesions. These differences suggest that hair loss partially requires DC activation.

In the lesions of patients with AA, HFs lost the IP upon IFN-γ upregulation, leading to ectopic MHC class I and II expression (52, 53). The MHC class I and II expression increase in parallel with the IFN-γ expression in AA mice (Fig. 1-3D, 3E, 4E) in good agreement with the clinical pathological data. Melanogenesis-related molecules (TYRP2, tyrosinase) and HF-specific proteins (trichohyalin and keratin 16/71/31) are potential AA autoantigens (23-25). However, it remains unclear if the autoantigens of the patients with AA are also the targets in this AA model. We investigated the possibility of melanogenesis-related molecules (TYRP2, tyrosinase) as autoantigens because we found that the AA mouse body hair partially whitened occasionally, indicating melanogenesis dysfunction (data not shown). Their mRNA expressions were lower in the lesions than in the non-lesions (Fig. 1-5A), indicating that infiltrating T cells attack melanocytes to downregulate melanogenesis and hair growth in the lesions. The TYRP2 and tyrosinase antibody serum levels increased in both unaffected and AA mice. Particularly, the anti-tyrosinase antibody titer robustly increased (Fig. 1-5B). Next, we investigated these antigen-specific T cells in the SDLNs of AA mice using MHC class I tetramer assay. The TYRP2- and tyrosinase-specific $CD8^+$ T cell percentages were upregulated in AA mice. The increase of the tyrosinase-specific $CD8^+$ T cells was particularly remarkable in parallel to the serum anti-tyrosinase antibody (Fig. 1-5C). These results indicate that AA mice exhibited cellular and humoral immune responses to TYRP2 and tyrosinase, suggesting that they are autoreactive targets in the AA model. The CTL response against tyrosinase in the PBMCs of patients with AA is reportedly higher than that against TYRP2 (23). The serum antibodies against these two antigens were detected in certain patients with AA (54). Taken together, these results suggest that the AA mouse model partially reflects the autoimmune responses of patients with AA.

In conclusion, we reported that upregulated memory T cell subpopulations in the LNs, PBMCs, and the skin of the AA mouse model differed between the acute and chronic phases. We also revealed that the cytokine, chemokine, and MHC class I/II expression levels in the lesions and non-lesions were different. Furthermore, TYRP2 and tyrosinase were directly identified as autoreactive targets in the AA mouse model. We consider that the AA mouse model reflects the pathological alterations between the different phases in

patients with AA. Therefore, the observations in this model could potentially lead to a better understanding of the development of AA in humans.

Chapter 2

Induction of alopecia areata in C3H/HeJ mice using cryopreserved lymphocytes*

*The content described in Chapter 2 was originally published in *Journal of Dermatological Science*. Hashimoto K, Yamada Y, Sekiguchi K, Matsuda S, Mori S, Matsumoto T. Induction of alopecia areata in C3H/HeJ mice using cryopreserved lymphocytes. *J. Dermatol. Sci.* 2021;**102**(3):177-183.

2.1 Introduction

Animal models are necessary to screen or identify candidate therapeutic agents. Twenty percent of female C3H/HeJ mice spontaneously develop AA-like hair loss by 18 months of age with variations in the occurrence and onset of hair loss (30). The transplant of full-thickness lesional skin grafts from AA-affected mice accelerated the incidence of hair loss and skin from a single AA donor mouse can be grafted onto 10-20 recipient mice (55). This method is useful but requires invasive surgery. Hence, there is a risk of infection and transplantation rejection. Recently, a new C3H/HeJ model was developed by the intradermal injection of cultured SDLN cells from AA-affected mice into naïve recipients (31, 32). LN cells were stimulated with recombinant IL-2 and magnetic beads coated with anti-CD3 and anti-CD28 antibodies to promote cell expansion. Although the number of SDLN cells from each AA-affected donor mouse is variable, more than 50 recipient mice can be transferred with expanded cells from a single AA donor. This model is useful because of its replicability and simplicity; however, this conventional method requires not only spontaneously AA-affected mice but also the continuous breeding of AA mice as donor mice, which is troublesome.

Therefore, to solve the troublesome matter, we investigated whether the use of cryopreserved LN cells from AA-affected mice was able to induce AA with a high incidence in naïve mice. To investigate whether the AA mice generated with this new method had similar pathological characteristics to AA mice generated with the conventional method and AA patients, we performed hematoxylin and eosin (H&E) staining and immunohistochemical staining, quantified the mRNA expressions of pro-inflammatory cytokines or chemokines, and measured cytokine production in hair loss skin. Moreover, to clarify which cell population contributed to AA development, we compared the cell profiles of transferred cells in the new method with that of the conventional method.

2.2 Materials and Methods

2.2.1 Mice and induction of AA

Female 7-week-old C3H/HeJ mice were obtained from Japan SLC, Inc. (Shizuoka, Japan). All mice were housed in specific-pathogen-free conditions. They received food pellets for long term breeding (CR-LPF; Oriental Yeast Co., Ltd., Tokyo, Japan) and ultraviolet sterile water *ad libitum*. All animal experiments were performed in accordance with the "Guiding Principles for the Care and Use of Animals in the Field of Physiological Sciences" of the Physiological Society of Japan. All animal experimental procedures were approved by the Ethics Committee for Animal Experiments of Maruho Co., Ltd. (Kyoto, Japan) and were conducted in accordance with the Guiding Principles for the Care and Use of Laboratory Animals at Maruho Co., Ltd.

The AA mouse model was induced by transferring *in vitro* expanded LN cells from AA-affected mice as described in chapter 1. For cell cryopreservation, cells were washed with phosphate-buffered saline (PBS; Sigma-Aldrich, St. Louis, MO, USA) and suspended in KM banker II (Kohjin Bio, Saitama, Japan). Cell tubes were stored at –80°C first and then transferred to liquid nitrogen storage. Thawed cells were cultured for 7 days as previously described.

2.2.2 Scoring of hair loss

To assess the severity of AA, an objective scoring system was developed according to the percentage of hair loss area. Hair loss was checked every 2 weeks after LN cells were transferred and was scored as follows: S0 (without hair loss, 0% hair loss), S1 (hair loss in less than half of the abdominal area, 1%-24% hair loss), S2 (hair loss in more than half of the abdominal area, 25%-49% hair loss), S3 (hair loss in the whole abdominal area and less than half of the dorsal area, 50%-74% hair loss), S4 (hair loss in the whole abdominal and more than half of the dorsal area, 75%-99% hair loss), and S5 (hair loss in the whole abdominal and the dorsal area, 100% hair loss) (56).

2.2.3 Flow cytometric analysis

For the staining of surface markers, single-cell suspensions were pre-incubated with anti-CD16/32 (Thermo Fisher Scientific) in MACS Buffer (autoMACS Rinsing Solution containing 0.5% bovine serum albumin; Miltenyi Biotec, Bergisch Gladbach, Germany) to block non-specific binding of antibodies to FcγR. Cells were incubated with fluorochrome-conjugated antibodies and stained with 7-AAD (eBioscience) to exclude non-viable cells. For the detection of intracellular markers, single-cell suspensions were first stained using LIVE/DEAD Fixable Aqua Dead Cell Stain Kit (Thermo Fisher Scientific) then pre-incubated with anti-CD16/32 and incubated with antibodies for surface markers. Subsequently, the cells were fixed and permeabilized using the Transcription Factor Buffer Set (BD Biosciences), and stained intracellularly.

Flow cytometric analysis was conducted using a FACSAria III (BD Biosciences). Fluorochrome-conjugated antibodies were as follows: CD3 (145-2C11, BD Biosciences), CD4 (GK1.5, BioLegend, San Diego, CA, USA), CD8 (53-6.7, BD Biosciences), NKG2D (CX5, eBioscience), CXCR3 (CXCR3-173, eBioscience), CCR4 (2G12, BioLegend), Streptavidin (BD Biosciences), CD44 (IM7, eBioscience), CD62L (MEL-14, eBioscience), CD25 (PC61.5, eBioscience), Foxp3 (FJK-16s, eBioscience), CD11c (HL3, BD Biosciences), Siglec-H (551.3D3, Miltenyi Biotec), and mPDCA-1 (JF05-1C2.4.1, Miltenyi Biotec). Cell populations were identified as follows: T_{EM} ($CD44^+CD62L^-$), T_{CM} ($CD44^+CD62L^+$), Th1 ($CD4^+CXCR3^+$), Th2 ($CD4^+CCR4^+$), Tc1 ($CD8^+CXCR3^+$), type 2 cytotoxic T cell (Tc2; $CD8^+CCR4^+$), regulatory T cell (Treg; $CD4^+CD25^+Foxp3^+$), and plasmacytoid dendritic cell (pDC; Siglec-H^+mPDCA-1^+).

2.2.4 Quantitative real-time PCR

Total RNA was isolated from homogenized skin samples of the lesional area using an RNeasy Fibrous Tissue Mini Kit (Qiagen). cDNA was synthesized by reverse transcription of total RNA using a High Capacity cDNA Reverse Transcription Kit (Thermo Fisher Scientific). Amplification was performed using the TaqMan Gene Expression Master Mix and TaqMan Gene Expression Assay (Thermo Fisher Scientific).

Primer sets purchased from Thermo Fisher Scientific were as follows: *B2m* (Mm00437762_m1), *Cxcl11* (Mm00444662_m1), *Gzmb* (Mm00442837_m1), *Ifng* (Mm01168134_m1), *Il2* (Mm00434256_m1) *Il13* (Mm00434204_m1), *Il17a* (Mm00439618_m1), *Stat1* (Mm01257286_m1), and *Gapdh* (Mm99999915_g1). The results were normalized to *Gapdh* and analyzed with QuantStudio 7 Flex Real-Time PCR Systems and StepOnePlus System (Thermo Fisher Scientific).

2.2.5 ELISA

Skin samples were homogenized in PBS containing 0.1% Tween 20 (Nacalai Tesque) and a 1% Protease Inhibitor Cocktail Set III (Merck, Darmstadt, Germany) and centrifuged at 10,000 × *g* at 4°C for 10 min. The concentration of multi-subtype IFN-α in the supernatants was measured using a VeriKine-HS Mouse IFN-α All Subtype ELISA Kit (PBL Assay Science, Piscataway, NJ, USA).

2.2.6 H&E staining

Skin samples were collected and fixed in 10% formalin. Paraffin embedded sections (5 μm) were stained with H&E. The stained slides were subsequently evaluated under an inverted microscope (Olympus) and imaging software cellSens (Olympus).

2.2.7 Immunohistochemical staining

Frozen skin sections (8 μm) were fixed in methanol/acetone (1:1) or acetone (–20°C) and stained with primary antibodies: anti-CD8α-biotin (53-6.7, Biolegend) and anti-NKG2D-PE (CX5, eBioscience). Alexa Fluor 488-conjugated streptavidin (Thermo Fisher Scientific) was used as secondary antibody. Hoechst 33,342 (Thermo Fisher Scientific) was used for nuclear staining. Images were obtained by a confocal laser scanning microscope (Olympus).

2.2.8 Statistical analysis

Data are expressed as the mean ± SE. Statistical analysis was conducted using Dunnett's multiple comparison test, as implemented in EXSUS (CAC Croit, Tokyo, Japan). *P*-values less than 0.05 were considered statistically significant.

2.3 Results

2.3.1 Transfer of cryopreserved cells induces AA in C3H/HeJ mice

We investigated whether the transfer of cryopreserved cells induced AA in C3H/HeJ mice. First, SDLN cells (Fig. 2-1A ‡1) were obtained from AA-affected mice and cultured for 7 days (Fig. 2-1A ‡2). Expanded cells were cryopreserved and transferred into naïve mice soon after thawing (Fig. 2-1A §1). About 50% of mice started developing AA from 12 weeks after cell transfer; however, the hair loss scores of most mice were S0 to S1 even at 20 weeks post-cell transfer (Fig. 2-1B §1). However, in the conventional method, some mice developed AA symptoms 4 weeks after cell transfer. More than 80% of mice developed AA and half of the mice advanced to S3 at 20 weeks post-cell transfer. These findings demonstrated that the onset of AA was delayed and the incidence and severity of AA also decreased with the cryopreserved method (§1) compared with the conventional method.

Furthermore, we attempted to proliferate thawed cells (Fig. 2-1A ‡3), because cell viability after thawing were more than 70%. However, the number of cells from all three donors was decreased by 50% after 7 days of culture (data not shown), and then we did not transfer the cells into mice.

Last, SDLN cells were cryopreserved soon after they were isolated from AA-affected mice. Thawed cells were cultured for 7 days (Fig. 2-1A ‡4), expanded fifty-fold, and transferred into naïve mice (Fig. 2-1A §2). Several mice developed AA symptoms from 6 weeks after cell transfer and the incidence increased to more than 90% at 20 weeks post-cell transfer (Fig. 2-1B §2). We confirmed the reproducibility of the incidence and severity of AA using cryopreserved cells isolated from more than five donor mice (data not shown).

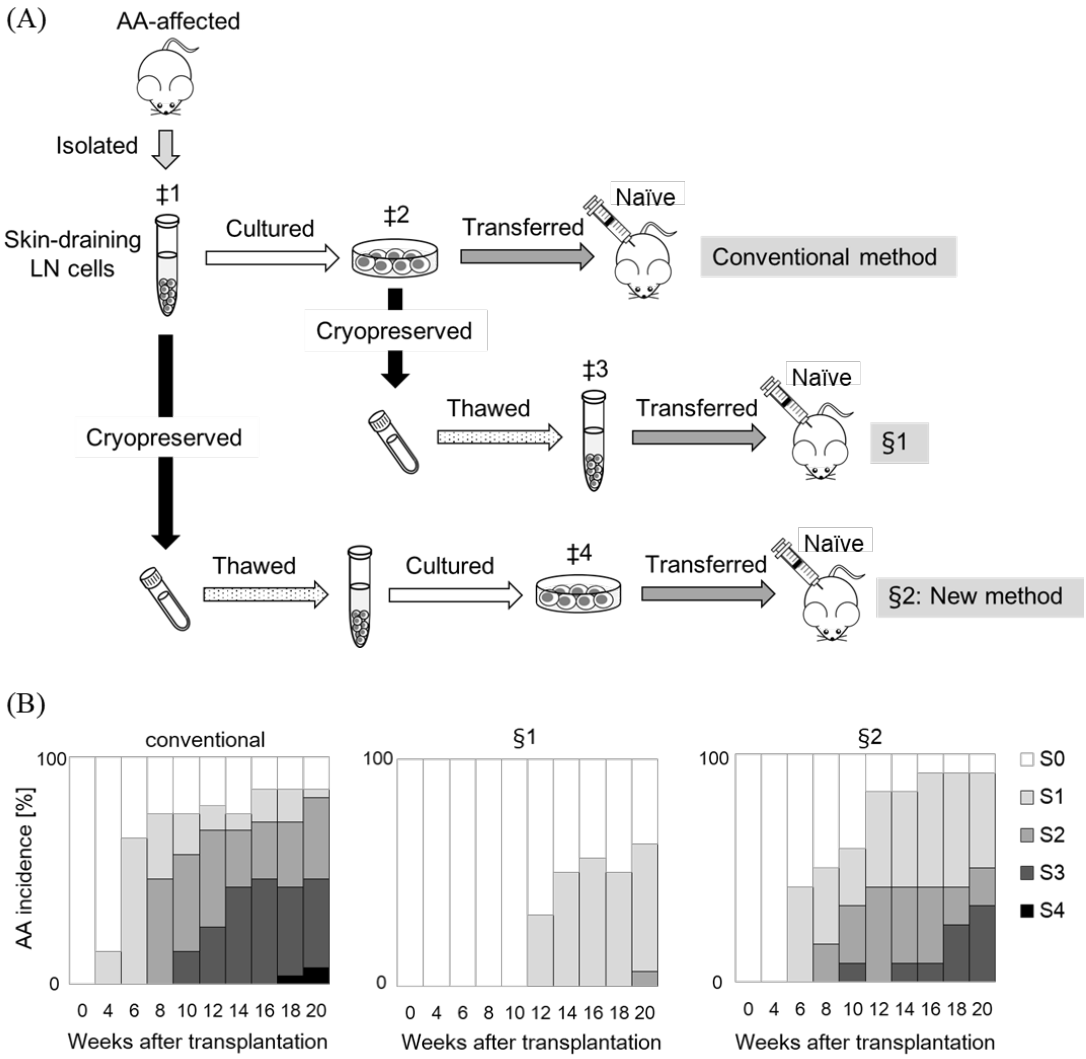

Fig. 2-1. AA mice induced by cryopreserved LN cells.

(A) The scheme shows methods for generating AA mice. In the conventional method (N = 28), isolated SDLN cells were cultured and transferred to naïve C3H/HeJ mice. In §1 (N = 16), cultured cells from the conventional method were cryopreserved. After thawing, cells were transferred to naïve C3H/HeJ mice. In §2 (the new method) (N = 12), isolated SDLN cells were cryopreserved. After thawing, cells were cultured and transferred to naïve C3H/HeJ mice. (B) Hair loss was scored every 2 weeks after LN cells were transferred according to the percentage of hair loss area. S0, 0%; S1, 1%-24%; S2, 25%-49%; S3, 50%-74%; S4, 75%-99%; S5, 100%.

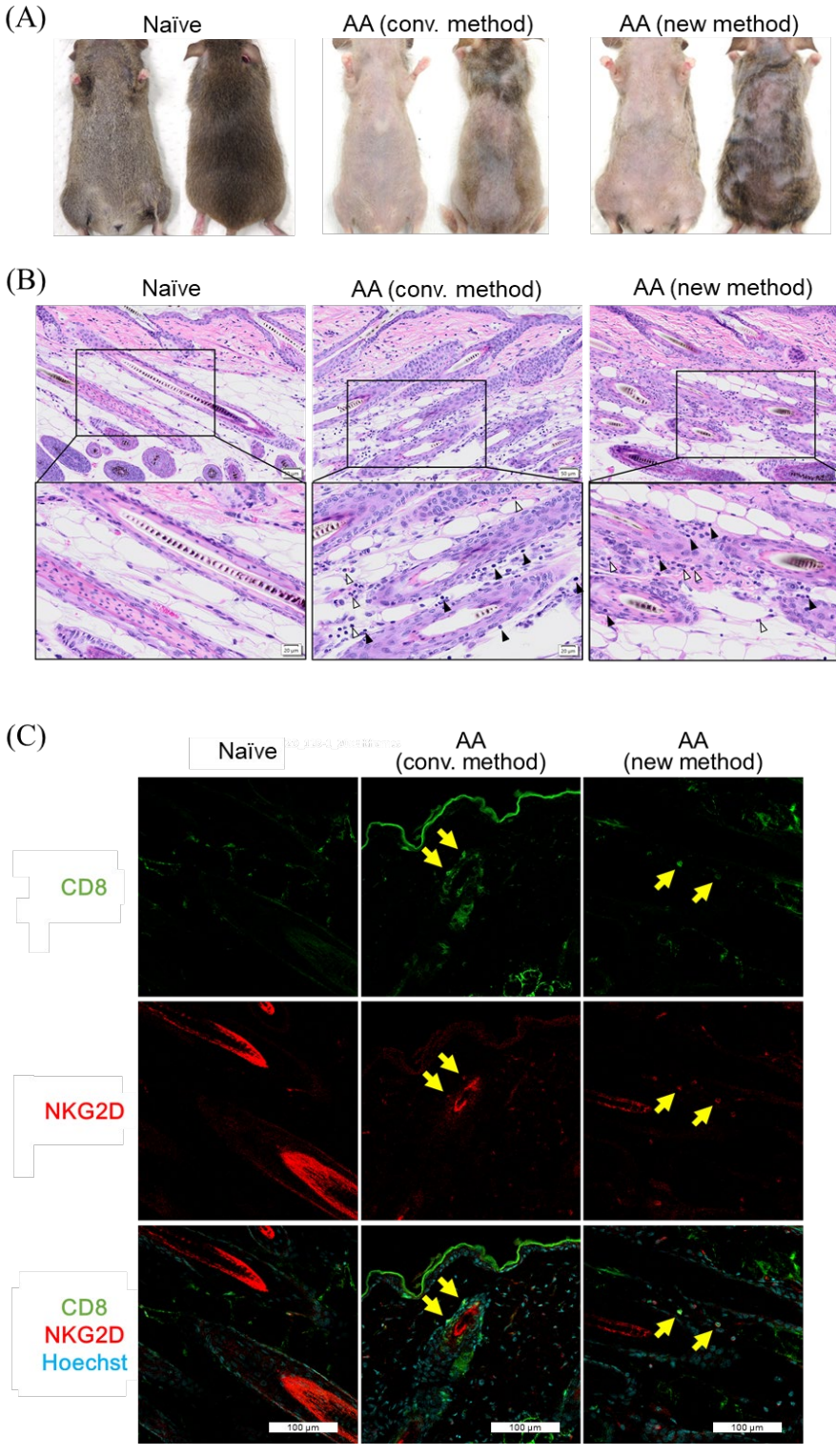
(A)
Naïve
AA (conv. method)
AA (new method)
(B)
Naïve
AA (conv. method)
AA (new method)
(C)
Naïve
AA
(conv. method)
AA
(new method)
CD8
NKG2D
CD8
NKG2D
Hoechst
100 μm
100 μm
100 μm

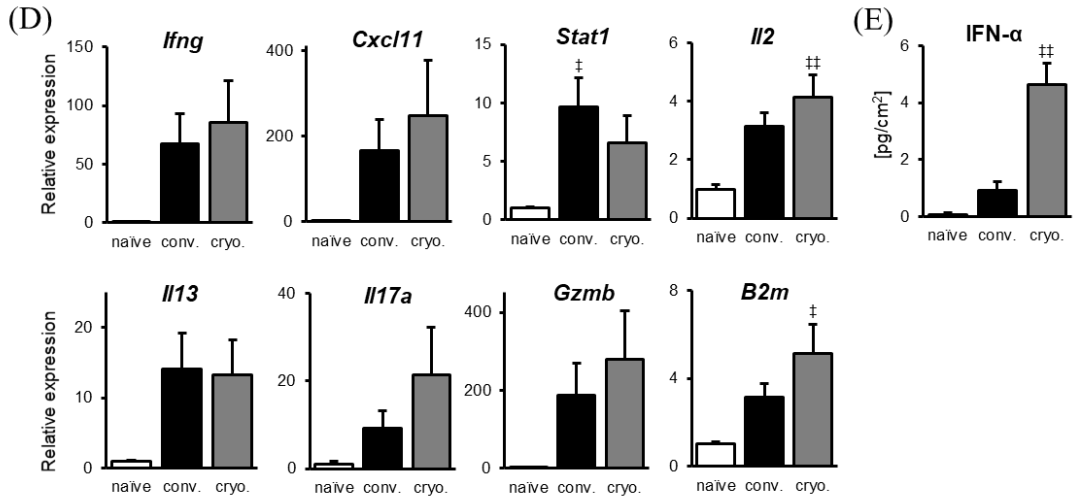

Fig. 2-2. Pathologic features of AA mice induced by cryopreserved LN cells.

(A) Representative images of AA mice induced by cryopreserved cells (new method; Fig. 2-1 §2) or fresh cells (conventional method) and naïve mice. (B) H&E staining of the skin from a naïve mouse and AA mice (conventional and new method). Lymphocytes are marked with black arrows. Neutrophils are marked with white arrows. (C) Immunohistochemical staining of the skin from a naïve mouse and AA mice (conventional and new method). $CD8^+NKG2D^+$ cells are marked with yellow arrows. (D) mRNA expressions (*Ifng*, *Cxcl11*, *Stat1*, *Il2*, *Il13*, *Il17a*, *Gzmb*, *B2m*) in the skin were analyzed by RT-qPCR. (E) Protein levels of multi-subtype IFN-α in the skin were measured by ELISA. Data are expressed as the mean ± SE (N = 4-5). Dunnett's multiple comparison test. (‡$p < 0.05$, ‡‡$p < 0.01$ vs naïve mice).

2.3.2 Characteristics of AA mice induced by cryopreserved cells reflects AA

AA mice induced with the new method developed hair loss symptoms (Fig. 2-2A) with a similar phenotype to those of AA mice induced with the conventional method. We examined the pathological changes in AA mice induced with the new method using cryopreserved cells compared with AA mice induced with the conventional method using fresh cells. Compared with naïve mice, infiltration of inflammatory cells such as lymphocytes and neutrophils, and $CD8^+NKG2D^+$ T cells was increased around anagen HFs in the skin of AA mice induced by cryopreserved cells, similar to that in AA mice

induced with the conventional method (Fig. 2-2B, C). We also examined the mRNA and protein expressions of cytokines and chemokines in the skin. A marked increase in the mRNA expressions of Th1-related markers (IFN-γ, CXCL11, and STAT1), IL-13, IL-17A, IL-2, granzyme B, and β2-microglobulin was observed in AA mice induced by fresh cells and cryopreserved cells compared with naïve mice (Fig. 2-2D). IFN-α protein levels were also significantly increased in AA mice compared with naïve mice (Fig. 2-2E).

2.3.3 T_{EM} cells and DCs may contribute to AA development

To clarify which cell population contributed to developing AA, we performed flow cytometric analysis in each step of the conventional method, §1 method (Fig. 2-1A) and the new method (§2; Fig. 2-1A) (‡1~‡4; Fig. 2-1A). Seven days of culture doubled the percentage of $CD8^+$ T_{EM} cells reaching more than 50% of $CD3^+$ T cells (Fig. 2-3A ‡1 vs ‡2). After thawing cells, the percentage of $CD8^+$ and $CD4^+$ T_{EM} cells were markedly decreased (Fig. 2-3A ‡2 vs ‡3), and consequently, ‡3 cells failed to induce high AA incidence. The $CD8^+$ T_{EM} cell percentage in transferred cells of the new method exceeded 60% (Fig. 2-3A ‡4), similar to the percentage in transferred cells of the conventional method (Fig. 2-3A ‡2). The $CD8^+$ T_{CM} and $CD4^+$ T_{EM} cell percentages were greater in transferred cells of the conventional method and the new method (high AA incidence) compared with transferred cells from §1 (low AA incidence) (Fig. 2-3A ‡2, ‡3, ‡4). The percentage of $NKG2D^+$ Tc1 cells was greater in ‡4 (13.6%) compared with ‡3 (0.2%), but that of ‡2 (0.9%) was similar to that of ‡3 (Fig. 2-3B). There was no correlation between the percentage of $NKG2D^+$ Tc1 cells in the transferred cells and AA incidence. The Treg percentage in ‡3 (1.4%) was lower than that in ‡2 (3.0%) (Fig. 2-3B). The percentages of $CD11c^+$ DCs (‡2: 2.9%, ‡3: 1.4%, ‡4: 2.2%) were greater in ‡2 and ‡4 cells (high AA incidence) compared with ‡3 cells (low AA incidence) (Fig. 2-3C). Freeze-thawing and culturing reduced the percentage of pDCs. ‡4 cells inducing high AA incidence did not contain pDCs.

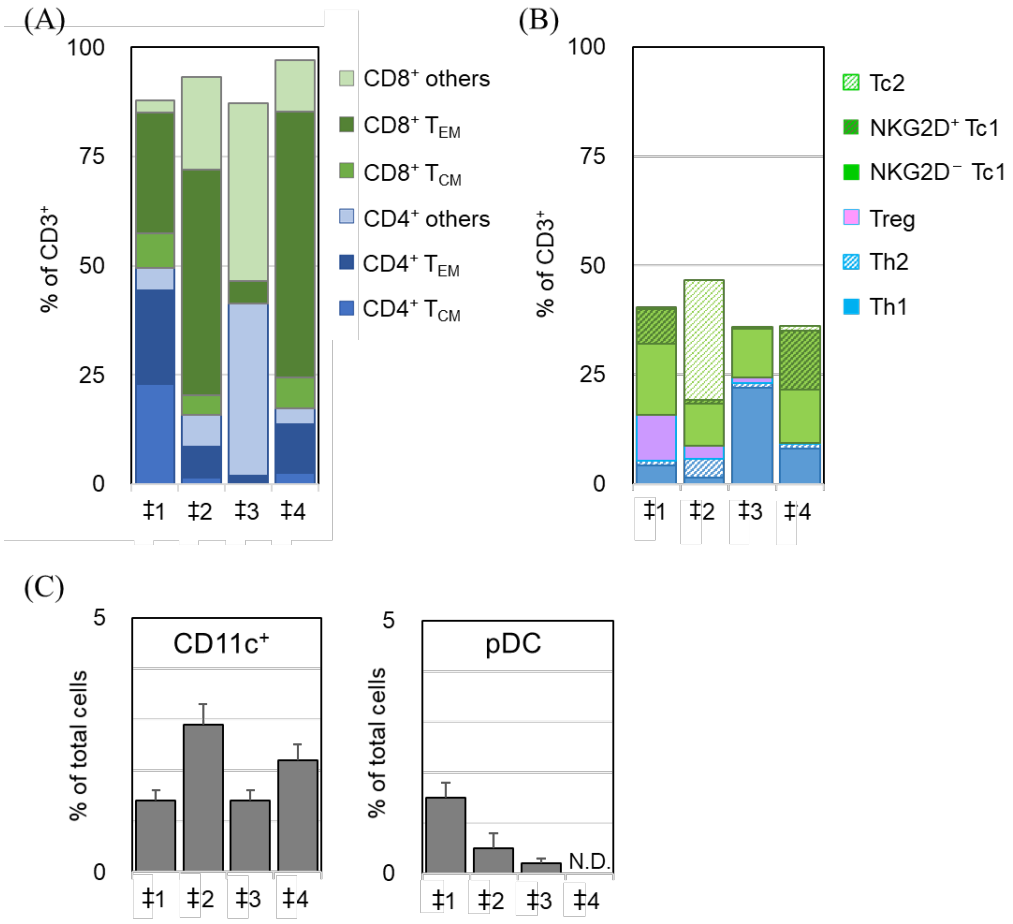

Fig. 2-3. Cell population analysis of transferred cells in each step.
Flow cytometric analysis was performed to profile the transferred cells shown in Fig. 2-1 (‡1, isolated SDLNs from AA-affected mice; ‡2, transferred cells of the conventional method; ‡3, transferred cells of §1; ‡4, transferred cells of the new method). (A, B) The percentages of T_{EM} ($CD44^+CD62L^-$), T_{CM} ($CD44^+CD62L^+$), Th1 ($CD4^+CXCR3^+$), Th2 ($CD4^+CCR4^+$), Treg ($CD4^+CD25^+Foxp3^+$), Tc1 ($CD8^+CXCR3^+$), and Tc2 ($CD8^+CCR4^+$) compared to $CD3^+$ T cells were calculated. (C) The percentage of $CD11c^+$ DCs and pDCs (Siglec-H^+mPDCA-1^+) were assessed. N.D., not detected. Data are expressed as the mean ± SE (N = 3).

2.4 Discussion

The AA animal model is useful for identifying candidate therapeutic agents. Recently, a new C3H/HeJ model was developed by the adoptive transfer of cultured lymphoid cells from spontaneously AA-affected mice (31). This method makes it easier to generate AA mice but requires their continuous breeding.

In this study, we attempted to generate AA-affected mice using cryopreserved cells. By cryopreserving lymphoid cells soon after their isolation from AA mice and transferring the cells to naïve mice, we succeeded in reproducing the AA mouse model. The AA incidence and severity of mice transferred with cryopreserved lymphoid cells were similar to those of AA mice generated with the conventional method (Fig. 2-1). We also noticed that there was a variation in the incidence and severity of AA in both the conventional method and the new method, which might be due to the difference in the cell population of SDLNs between donors. As for the conventional method, in this study, 83% of recipients reached S2/S3/S4 severity 20 weeks after cell transfer (Fig. 2-1B). In another one, about 40% of recipients reached S2/S3 severity (data not shown). As for the new method, in this study, S2/S3 incidence was 50% 20 weeks after cell transfer (Fig. 2-1B §2). In another one, S2/S3 incidence was more than 75% (data not shown). In the new method, thawed cells were expanded about fifty-fold over 7 days of culture and more than 50 recipient mice could be transferred with expanded cells, similar to the expansion rate of fresh cells in the conventional method (data not shown). The cell storage solution we used was for lymphoid cell lines. We speculate this optimal choice is a key in the new method. Furthermore, we revealed that AA mice generated using cryopreserved cells with the new method can be used as donors (data not shown). S4 mice appeared at 26 weeks after cell transfer (data not shown) and those mice can be used as donors with the conventional method or the new method. However, cryopreservation after culture markedly reduced the AA incidence and severity (Fig. 2-1 §1), suggesting that the cryopreserving and thawing procedure lost proliferative activity.

The present study showed that the pathophysiological characteristics of AA mice generated with the new method were similar to AA mice induced by fresh cells with the conventional method. In AA mice generated by the new and conventional methods, higher

numbers of inflammatory cells were present in perifollicular areas of anagen hair compared with naïve mice (Fig. 2-2B). In AA mice generated by the new method as well as AA mice generated by the conventional method, $CD8^+NKG2D^+$ T cells were infiltrated around HFs (Fig. 2-2C). In healthy donors, IP of the HF is achieved by the downregulation of MHC class I and β2-microglobulin, followed by the repression of intra-follicular antigen-presenting cells, perifollicular NK cells, and mast cells (17, 19). However, anagen HFs in AA patients have perifollicular infiltrations of $CD4^+$, $CD8^+$ T cells, mast cells, and Langerhans cells, and the abnormal expression of MHC class I and II molecules (17, 19, 57). Pathological features of AA mice generated with the new method and the conventional method are in accordance with those of AA patients. The upregulation of β2-microglobulin and granzyme B mRNA expression in AA mice (Fig. 2-2D) indicated a high expression of MHC class I and cytotoxic lymphocyte infiltration, suggesting the collapse of the IP around HFs. Th1- (IFN-γ, CXCL11, STAT1), Th2- (IL-13), and Th17-related (IL-17A) markers were all increased in the skin of AA mice (Fig. 2-2D). The expressions of IFN-γ and CXCL11 were dominantly increased compared with IL-13 and IL-17A (Fig. 2-2D), indicating Tc1 or Th1 were predominant among T cell subsets that had infiltrated around the anagen HFs. It was reported that more than 80% of infiltrating $CD4^+$ T cells around the HFs of AA patients were $CCR5^+$ and 10% of $CD4^+$ T cells were $CCR4^+$, suggesting Th1 reactions are dominant in AA lesions (58). Our results regarding the involvement of Th1/Th2 in the pathophysiology of AA mice are consistent with the clinical features in AA patients. RT-qPCR profiling data of AA patients showed that Th1 markers (IFN-γ, CXCL9, CXCL10), Th2 markers (IL-13, IL-10, CCL5), and IL-23 (IL-23p19, IL-12/IL-23p40) were highly increased in AA lesions, whereas Th17/Th22 cytokines (IL-17A, CCL20, IL-22) were not increased (38). In contrast, studies reported that IL-17 and IL-22 protein levels in AA lesions were significantly higher compared with healthy controls (59) and that Th17 infiltration was observed around HFs in all AA cases (60). These latter reports are in accord with our findings in AA mice. Recently, in addition to T cells, pDCs were proposed to have an important role in AA pathogenesis (61). Skin IFN-α protein levels were upregulated in AA mice (Fig. 2-2E), indicating activated pDCs infiltrated around HFs. This is in concordance with a report where pDCs were present in

the peribulbar areas of AA patients (62). Therefore, AA mice generated with the new method exhibit a phenotype and pathogenesis similar to that in AA patients.

Finally, we compared the cell profiles of transferred cells of the new method with that of the conventional method to clarify which cell population contributed to AA development. The percentages of $CD8^+$ T_{EM} cells were increased up to more than 60% of $CD3^+$ T cells in both methods (Fig. 2-3A). In contrast, the cell populations in ‡3 cells were very low and the cells failed to induce high AA incidence and severity (Fig. 2-1 §1). These data suggest that $CD8^+$ T_{EM} cells have an important role in AA development. The phenotype of skin-infiltrating $CD8^+$ T cells in AA mice was similar to that of SDLN cells and most were $CD8^+CD44^{hi}CD62L^{lo}CD103^+$-bearing NK immune-receptors (34). Administration of suppressors of cytokine signaling 3 protein prevented the onset of AA in mice by decreasing $CD8^+$ T_{EM} cells and IFN-γ production (63), suggesting the importance of $CD8^+$ T_{EM} cells in AA development. In addition to memory $CD8^+$ T cells, memory $CD4^+$ T cells are also thought to have an important role in AA development. Injection of non-cultured $CD4^+$ T cells alone was enough to induce AA (64). In our experiment, hair loss began at axillary abdominal skin and expanded to total abdomen skin. The results suggest that antigen-specific memory $CD4^+$ cells stimulate naïve and $CD8^+$ cells via antigen-presenting cells at axillary LNs and educated T cells attack HFs.

$CD8^+NKG2D^+$ T cells were reported to infiltrate the HFs of AA patients and skin-grafted AA mice (34), indicating they might contribute to AA pathogenesis. This report also demonstrated that the transfer of $NKG2D^+$ cell-depleted LN cell populations did not induce AA. $CD8^+NKG2D^+$ T cells are thought to be the dominant cell type in dermal infiltration and to be necessary for the induction of AA in mice by cell injection. Furthermore, $CD8^+$ T cells in the LN of AA mice expressed high levels of IFN-γ, suggesting Tc1 cells are critical for AA among $CD8^+$ T cells. This hypothesis is supported by a report showing that IFN-inducible chemokine receptor, CXCR3 blockade prevented the development of AA by inhibiting T cell migration into the skin (43). In the current study, no correlation between the percentage of $NKG2D^+$ Tc1 cells and AA development was observed (Fig. 2-3B). In §1 that failed to induce AA, the percentage of $NKG2D^+$ Tc1 cells was less than 1%, but was greater than 10% in the new method, which induced high

AA incidence and severity. However, the percentage of $NKG2D^+$ Tc1 cells in the conventional method was also less than 1%. Therefore, the contribution of $NKG2D^+$ Tc1 cells to AA development might be less important than that of $CD8^+$ T_{EM} cells.

Because little has been reported on the role of minor cell subsets, we investigated the contribution of $CD11c^+$ DCs and pDCs to the development of AA. Our data showed that the percentage of $CD11c^+$ in transferred cells correlated with AA incidence and severity in recipient mice. The results suggest that $CD11c^+$ may promote hair loss with assistance from T cells, although the transfer of $CD11c^+$ cells alone was reported to not induce localized or systemic AA hair loss (64). Our data revealed that the transfer of cells without pDC induced AA, although pDCs are still likely to be important in AA pathogenesis (61). Further research is needed to elucidate the role of these minor cell subsets in AA.

In conclusion, we report a new method to induce AA in mice using cryopreserved cells, which allows the generation of large numbers of AA mice with a high frequency as needed. Our data demonstrated that the pathological characteristics of AA mice were similar to those of AA patients including inflammatory cell infiltration around anagen HFs and the upregulated expressions of cytokines and chemokines. Moreover, our findings suggest that T_{EM} cells and $CD11c^+$ DCs contribute to the induction of AA. This method is expected to be very useful for AA research and the preclinical screening of therapeutic candidates with convenience and high reproducibility.

Chapter 3

NLRP3 inflammasome activation contributes to development of alopecia areata in the C3H/HeJ mouse model*

*The content described in Chapter 3 was originally published in *Experimental Dermatology*.
Hashimoto K, Yamada Y, Sekiguchi K, Mori S, Matsumoto T. NLRP3 inflammasome activation contributes to development of alopecia areata in C3H/HeJ mice. *Exp. Dermatol*. 2022;**31**(2):133-142.

3.1 Introduction

In pathology of AA, what triggers IP collapse is still under debate. Several studies have indicated that the innate immune system plays an important role in the pathogenesis of AA, based on clinical reports concerning associations with viral infection (65-67), psychological stress (68), and oxidative stress (69). In innate immunity, pattern recognition receptors (PRRs), such as toll-like receptors (TLRs) and NLRP3, are key regulators. Activation of PRR signaling is essential for host defense against infection, whereas overactivation of PRRs often causes uncontrolled inflammation and autoimmune diseases (70, 71).

TLRs have been identified from TLR1 to TLR11 in humans. Several TLRs are localized in the endosome to detect nucleic acids derived from bacteria, viruses, and damaged cells. Endogenous nucleic acids, which are not recognized by the endosomal TLRs under homeostatic conditions, activate the TLRs and trigger development of autoimmune diseases (70) such as systemic lupus erythematosus (SLE) (72), rheumatoid arthritis (RA) (73), diabetes mellitus (74), psoriasis (75), and systemic sclerosis (SSc) (76). In AA patients, expressions of TLRs 3, 7, 8, and 9 are reported to be upregulated in PBMCs (77, 78) and/or around lesional HFs (78). Stimulation of TLRs 7 and 9 mediates IFN-α secretion from pDCs. pDCs are present in the peribulbar area of AA patients (62), and type 1 IFN inducible myxovirus protein A is expressed in AA lesions (79). A recent study showed that IFN-α-producing pDCs were infiltrated around HFs not only in AA lesions but also in non-lesional areas of AA-affected C3H/HeJ mice, and that intradermal injection of pDCs induced AA lesions in normal C3H/HeJ mice (61). IFN-α-producing pDCs are known to play a role in scarring alopecia such as Lupus erythematosus-associated alopecia (80).

NLRP3 is activated via the P2X7 receptor, assembling with apoptosis-associated speck-like protein containing a caspase recruitment domain (ASC), and pro-caspase-1 into inflammasomes. The NLRP3 inflammasome promotes secretion of IL-1β and IL-18. Several studies have revealed their significance in autoimmune disorders such as SLE, RA, and SSc (71). In AA patients, NLRP3 inflammasome components and IL-1β are reported to be highly expressed in the outer root sheath of HF (81). Serum levels of

IL-18 in patients with extensive AA are significantly higher than in healthy controls (82), and single-nucleotide polymorphisms in *Il18* (re187238 and rs549908) are related to the susceptibility to AA in Koreans (83).

Thus, several studies have suggested a contribution of IFN-α-producing pDCs and NLRP3 inflammasome activation to AA pathogenesis. However, their roles in the initiation of AA are yet to be clarified. To define their roles in the onset of AA, we investigated the expression of IFN-α and NLRP3-related factors, comparing before and after AA onset, using an AA mouse model reflecting AA pathogenesis (27). Furthermore, we studied the therapeutic effect of an NLRP3 inhibitor on AA. We demonstrate for the first time that inhibition of NLRP3 inflammasome may be a promising therapeutic approach to AA.

3.2 Materials and Methods

3.2.1 Mice and induction of AA

Female 7-week-old C3H/HeJ mice were obtained from Japan SLC (Shizuoka, Japan). All mice were housed in specific-pathogen-free conditions. They received food pellets for long term breeding (CR-LPF; Oriental Yeast, Tokyo, Japan) and ultraviolet sterile water *ad libitum*. All animal experimental procedures were approved by the Ethics Committee for Animal Experiments of Maruho (Kyoto, Japan) and conducted in accordance with the Guiding Principles for the Care and Use of Laboratory Animals at Maruho.

The AA mouse model was induced by transferring *in vitro* expanded LN cells from AA-affected mice as described in chapter 1. Mice were divided into the following four groups (N = 4 per group): naïve mice (without transferred LN cells); unaffected mice (with transferred LN cells but without hair loss); AA mice in the acute phase (with hair loss localized in less than half of the abdominal area for less than 2 weeks); AA mice in the chronic phase (with hair loss in whole abdominal area and less than half of dorsal area for more than 4 weeks).

3.2.2 MCC950 treatment

Among AA-affected mice in the acute phase (hair growth index between 50 and 100), mice were randomized into two groups: MCC950-treated or PBS-treated mice (N = 5 per group). Mice were injected intraperitoneally with MCC950 (20 mg/kg) (Selleck Chemicals, Houston, TX, USA) or PBS (Sigma-Aldrich) on days 0, 1, 3, 6, 8, 10, 13, 15, 17, 20, 22, 24, 27, 29, 31, 34, 36, 38, and 41. Hair growth was evaluated every week after the first administration. For analysis of pathological characteristics, mRNA expressions in skin, and cytokine productions in serum, AA-affected mice were injected intraperitoneally with MCC950 or PBS on days 0, 1, 3, and 6 (N = 3 per group).

3.2.3 Evaluation of hair growth

Hair growth was assessed in the square area (2 cm × 3 cm) on abdominal skin. Hair growth was evaluated using the 4-point score with definition as follows: 0 (no hair); 1 (non-dense short hairs); 2 (non-dense intermediate length hairs); and 3 (normal length and density hairs). The percentage of the area with each score point in 2 cm × 3 cm area was measured using ImageJ software (National Institutes of Health, Bethesda, MD, USA). Hair growth index was calculated as the sum of multiplying each hair growth score by the percentage of scored area.

3.2.4 Quantitative real-time PCR

Total RNA was isolated from homogenized skin samples (lesions, hair loss areas; non-lesions, normal hairy areas remote from lesions) using an RNeasy Fibrous Tissue Mini Kit (Qiagen, Germantown, MD, USA). cDNA was synthesized by reverse transcription of total RNA using High Capacity cDNA Reverse Transcription Kit (Thermo Fisher Scientific). Amplification was performed using TaqMan® Gene Expression Master Mix and TaqMan Gene Expression Assay (Applied Biosystems™, Waltham, MA, USA). The primer sets purchased from Thermo Fisher Scientific were as follows: *Ager* (Mm01134790_g1), *Casp1* (Mm00438023_m1), *Cxcl9* (Mm00434946_m1), *Cxcl10* (Mm00445235_m1), *Cxcl11* (Mm00444662_m1), *Gzmb* (Mm00442837_m1), *Hspa1a*

(Mm01159846_s1), *Hmgb1* (Mm00849805_gH), *Ifng* (Mm01168134_m1), *Irak4* (Mm00459443_m1), *Irf7* (Mm00516793_g1), *Nlrp3* (Mm00840904_m1), *Pycard* (Mm00445747_g1), *Traf3* (Mm00495752_m1), and *Gapdh* (Mm99999915_g1). The results were normalized to GAPDH and analyzed with QuantStudio 7 Flex Real-time PCR Systems and StepOnePlus system (Thermo Fisher Scientific).

To determine microRNA expressions, total RNA was extracted from whole blood using mirVana™ PARIS kit (Thermo Fisher Scientific). cDNA was synthesized using TaqMan™ Advanced miRNA cDNA Synthesis Kit. Amplification was performed using TaqMan Fast Advanced Master Mix and TaqMan Advanced miRNA Assay. The primer sets purchased from Thermo Fisher Scientific were as follows: *mmu-miR-30b-3p* (mmu481756_mir), *mmu-miR-150-5p* (mmu480947_mir), and *mmu-miR-423-3p* (mmu478327_mir). The results were normalized to *mmu-miR-423-3p* and analyzed with the StepOnePlus System.

3.2.5 ELISA and multiplex

Skin samples were homogenized in PBS containing 0.1% Tween 20 (Nacalai Tesque) and 1% Protease Inhibitor Cocktail Set III (Merck, Darmstadt, Germany) and centrifuged. Blood samples were collected under anesthesia and serum was isolated after coagulation and centrifugation. The concentrations of IFN-α, heat shock protein 70 (HSP70), and IL-18 were measured by ELISA using VeriKine-HS Mouse IFN-α All Subtype ELISA Kit (PBL Assay Science), Mouse HSP70 ELISA kit (CUSABIO), and Mouse IL-18 SimpleStep ELISA kit (Abcam). The concentrations of IL-1β, IFN-γ, tumor necrosis factor (TNF)-α, and IL-17A were measured using Bio-Plex Multiplex Immunoassay System (Bio-Rad) with Bio-Plex Pro Mouse Cytokine IL-1β Set and Bio-Plex Pro Mouse Cytokine Th1/Th2 Assay (Bio-Rad).

3.2.6 Histological analysis

Skin samples from MCC950- and PBS-treated mice were collected and fixed in 10% formalin. Paraffin embedded sections (5 μm) were stained with H&E. The stained slides

were subsequently evaluated using an inverted microscope (Olympus) and cellSens imaging software (Olympus).

3.2.7 Statistical analysis

Data are expressed as mean ± SE. Statistical analysis was conducted using Student's *t*-test or Dunnett's multiple comparison test, implemented using EXSUS software (CAC Croit, Tokyo, Japan). *P*-values less than 0.05 were considered statistically significant.

3.3 Results

3.3.1 IFN-α signal pathway is activated in lesion in the acute phase

pDCs and NLRP3 inflammasome have been suggested to be initiation factors in AA. We first examined pDC activation by comparing the disease phases. The IFN-α level in serum and skin of AA mice with different disease phases was assessed using ELISA (Fig. 3-1A, B). IFN-α concentration in serum was detectable only in unaffected mice and chronic-AA mice. Whereas IFN-α levels in non-lesional areas of AA mice were as low as those of naïve and unaffected mice, IFN-α levels in lesions were increased compared with non-lesional areas. We also examined the expression of factors that are crucial for IFN-α production (Fig. 3-1C–E). mRNA expression of interferon regulatory factor 7 (IRF7) was higher in lesions of the acute-AA mice and non-lesional areas and lesions of the chronic-AA mice. Interleukin-1 receptor-associated kinase 4 (IRAK4) and tumor necrosis factor receptor-associated factor 3 (TRAF3) expressions in lesion of the acute-AA mice were increased, and mRNA expression of IRAK4 in non-lesional areas was higher than in lesions of the chronic-AA mice. These results demonstrate that the IFN-α signal pathway is locally activated in lesional areas in the acute phase.

IFN-α production via TLR7/9 in pDCs is activated via several signal pathways suggested to play an important role in several autoimmune diseases. A complex of high mobility group box-1 (HMGB1) and DNA binds to receptor for advanced glycation end-products (RAGE) and induces IFN-α production (84). HSP70 potentiates DNA-induced IFN-α production (84). To elucidate the trigger of pDC activation and IFN-α production,

we determined mRNA expressions of HMGB1, RAGE, and HSP70 (Fig. 3-1F–H). The expressions of HMGB1, RAGE, and HSP70 increased in lesions of the acute-AA mice, which was similar to IFN-α. Serum level of HSP70 was increased in the acute-AA mice (Fig. 3-1I) and the expression of *mmu-miR-30b-3p*, which is reported to inhibit HSP70 expression, was higher in blood of AA mice, and particularly elevated in the chronic-AA mice (Fig. 3-1J). Taken together, HMGB1/RAGE and HSP70 signal pathways were activated and IFN-α production was increased in lesions in the acute phase.

Fig. 3-1. IFN-α signal pathway is activated in lesions in the acute phase of AA

IFN-α levels in serum (A) and skin (B) from naïve, unaffected, acute-AA, and chronic-AA mice were measured by ELISA. mRNA expressions of IRF7 (C), IRAK4 (D), TRAF3 (E), HMGB1 (F), RAGE (G), and HSP70 (H) were assessed by RT-qPCR. (I) Serum HSP70 level was measured by ELISA. (J) Expression of *mmu-miR-30b-3p* in blood was assessed using RT-qPCR. Skin samples were collected from non-lesional areas (NL; normal hairy area) and lesions (L; hair loss area). Data are expressed as mean ± SE (N = 4). ‡$p < 0.05$. ‡‡$p < 0.01$. vs. naïve (Dunnett's multiple comparison test). N, naïve mice; U, unaffected mice; A, acute-AA mice; C, chronic-AA mice. N.D., not detected.

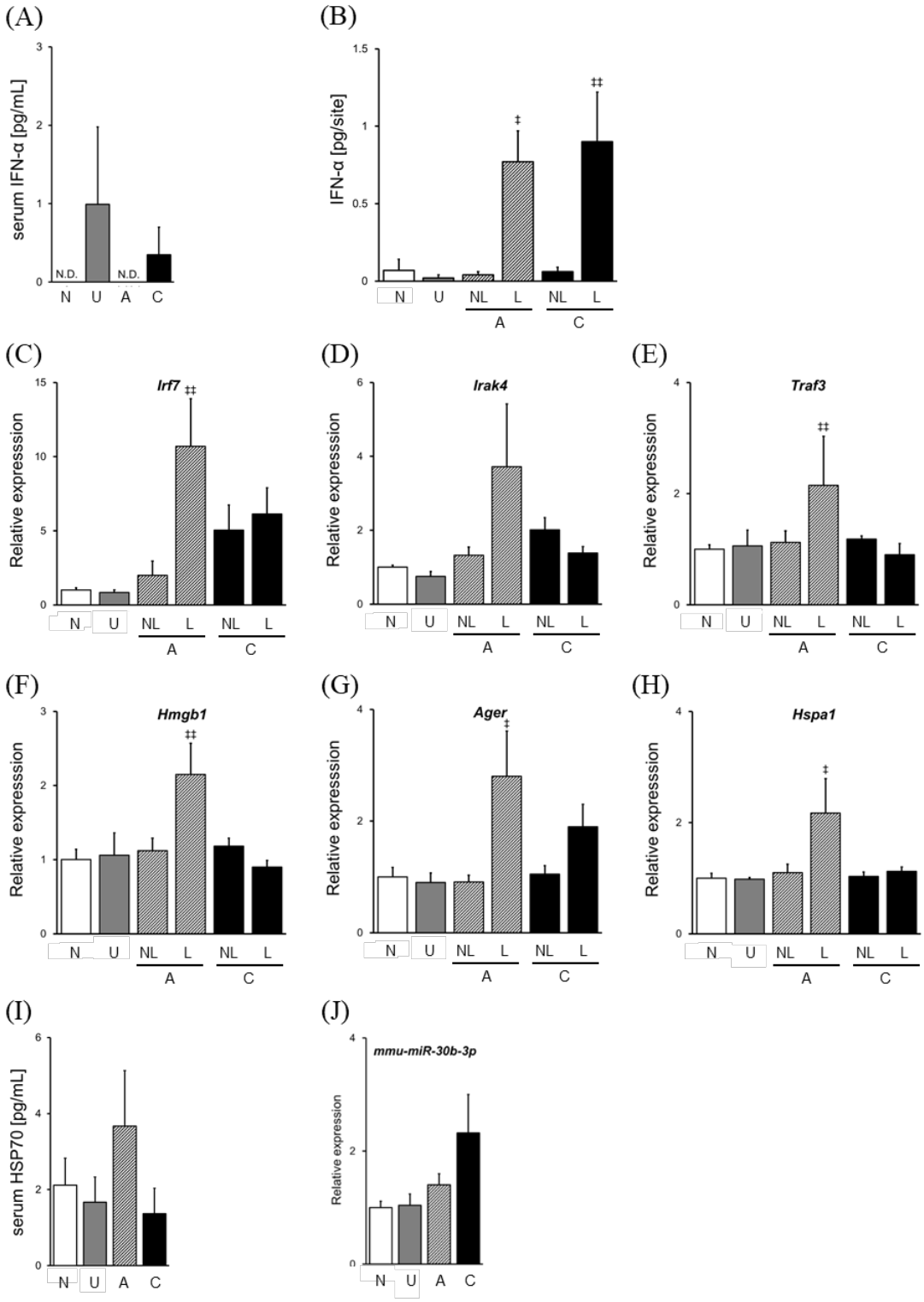
(A)
serum IFN-α [pg/mL]
N.D.
N.D.
N U A C
(B)
IFN-α [pg/site]
‡
‡‡
N U NL L NL L
A C
(C)
Irf7
‡‡
Relative expresssion
N U NL L NL L
A C
(D)
Irak4
Relative expresssion
N U NL L NL L
A C
(E)
Traf3
‡‡
Relative expresssion
N U NL L NL L
A C
(F)
Hmgb1
‡‡
Relative expresssion
N U NL L NL L
A C
(G)
Ager
‡
Relative expresssion
N U NL L NL L
A C
(H)
Hspa1
‡
Relative expresssion
N U NL L NL L
A C
(I)
serum HSP70 [pg/mL]
N U A C
(J)
mmu-miR-30b-3p
Relative expression
N U A C

3.3.2 NLRP3 Inflammasome signal pathway contributes to development and exacerbation of AA

Next, to investigate whether NLRP3 inflammasome contributes to AA development, we evaluated the production of IL-1β and IL-18 in serum and skin by comparing naïve, unaffected, acute-AA, and chronic-AA mice. Serum IL-1β level was subtly higher in unaffected and AA mice than in naïve mice (Fig. 3-2A). Serum IL-18 level was increased in the acute-AA mice and decreased in the unaffected and chronic-AA mice (Fig. 3-2B). Serum level of IFN-γ, that is reported to play a crucial role in the pathogenesis of AA, was significantly increased in the chronic-AA mice (Fig. 3-2C). The blood level of *mmu-miR-150-5p*, which is reported to inhibit IL-18 expression, was lower in the unaffected, acute-AA, and chronic-AA mice than in naïve mice (Fig. 3-2D). IL-1β production in skin was increased in the unaffected and AA mice, and the level was elevated depending on the progression of AA (Fig. 3-2E). IL-18 production was increased in non-lesional areas and lesions of AA mice, and the level was similar between the acute- and chronic-AA (Fig. 3-2F). Comparing IL-1β and IL-18 production, IL-18 level was significantly higher than IL-1β level both in serum and skin. Furthermore, IL-1β production, but not IL-18 production, was increased in the unaffected mice. These data demonstrate that IL-1β production increased before onset of AA, and IL-1β and IL-18 production increased in non-lesional areas as well as in lesions after onset. IFN-γ production in skin tended to increase in mice injected with LN cells compared to naïve mice (Fig. 3-2G). mRNA expressions of NLRP3 were increased both in non-lesional areas and lesions of the acute and chronic-AA mice, particularly in lesions of the acute-AA mice (Fig. 3-2H). mRNA expressions of NLRP3 inflammasome components, ASC (Pycard) and caspase-1, were increased in lesions of the acute-AA mice and non-lesional areas and lesions of the chronic-AA mice, and the level was similar between non-lesional areas and lesions in the chronic phase (Fig. 3-2I, J). These data demonstrate that NLRP3 inflammasome signaling in skin was activated in the acute phase and remained activated in the chronic phase, suggesting that NLRP3 inflammasome contributes to aggravation as well as onset of AA.

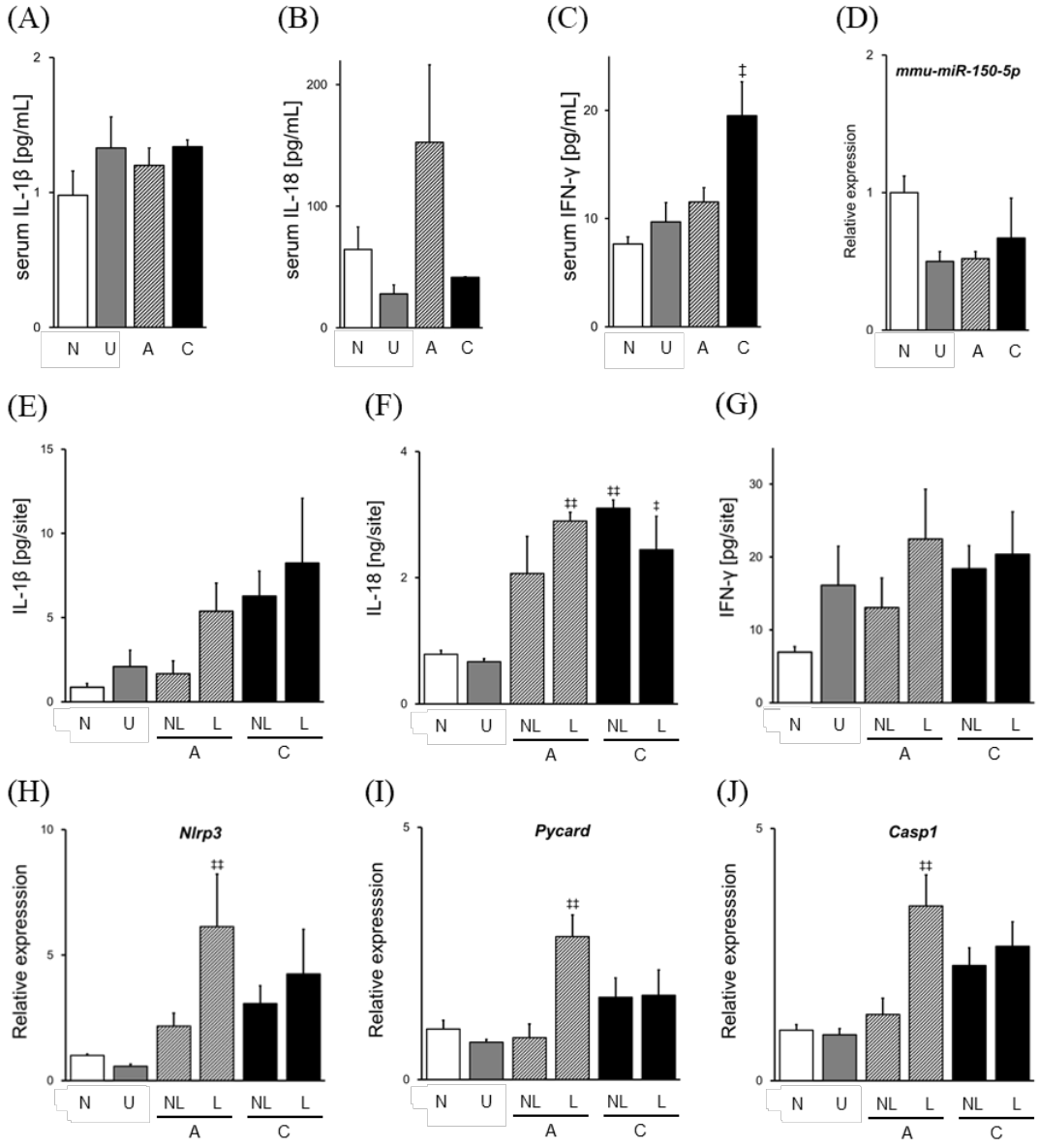

Fig. 3-2. Inflammasome signal pathway-related factors are increased in both the acute and chronic phases of AA

(A-C, E-G) IL-1β, IL-18, and IFN-γ levels in serum and skin from naïve, unaffected, acute-AA, and chronic-AA mice were measured by multiplex. (D) Expression of *mmu-miR-150-5p* in blood was assessed by RT-qPCR. (H-J) mRNA expressions of NLRP3, ASC, and caspase-1 in the skin were assessed by RT-qPCR. Data are expressed as mean ± SE (N = 4). ‡$p < 0.05$. ‡‡$p < 0.01$. vs. naïve (Dunnett's multiple comparison test). N, naïve mice; U, unaffected mice; A, acute-AA mice; C, chronic-AA mice.

3.3.3 NLRP3 inflammasome inhibitor MCC950 ameliorates AA in the mouse model

Finally, we investigated the therapeutic effect of a selective NLRP3 inflammasome inhibitor, MCC950, on AA in the mouse model. MCC950 or PBS was intraperitoneally injected into AA mice for 6 weeks. In MCC950-treated mice, hair growth was observed from 7 days up to 42 days after the first administration (Fig. 3-3A, B). Hair growth index increased from 81.1 ± 2.4 to 158.8 ± 34.0 in MCC950-treated mice, whereas it changed from 80.9 ± 5.4 to 86.4 ± 6.6 in PBS-treated mice.

As shown in Fig. 3-3B, the increase in hair growth index was observed even 7 days after the first MCC950 administration and was maintained up to 42 days. Therefore, to elucidate the effect of MCC950 on cytokines, chemokines, and NLRP3 inflammasome signaling in AA mice, we investigated pathological characteristics, mRNA expressions in the skin, and cytokine production in serum on day 7. H&E staining revealed that MCC950 treatment decreased infiltration of inflammatory cells such as neutrophils and lymphocytes (Fig. 3-4A). MCC950 treatment decreased mRNA expression of Th1/Tc1 chemokines (CXCL9/10/11), Th1/Tc1 cytokine (IFN-γ), and cytotoxic marker (granzyme B) in the skin (Fig. 3-4B). mRNA expressions of NLRP3 inflammasome-related factors (NLRP3, ASC, caspase-1) were reduced by MCC950-treatment (Fig. 3-4C). Serum levels of cytokines (IFN-γ, TNF-α, and IL-17A) were lower in MCC950-treated mice than in PBS-treated mice (Fig. 3-4D).

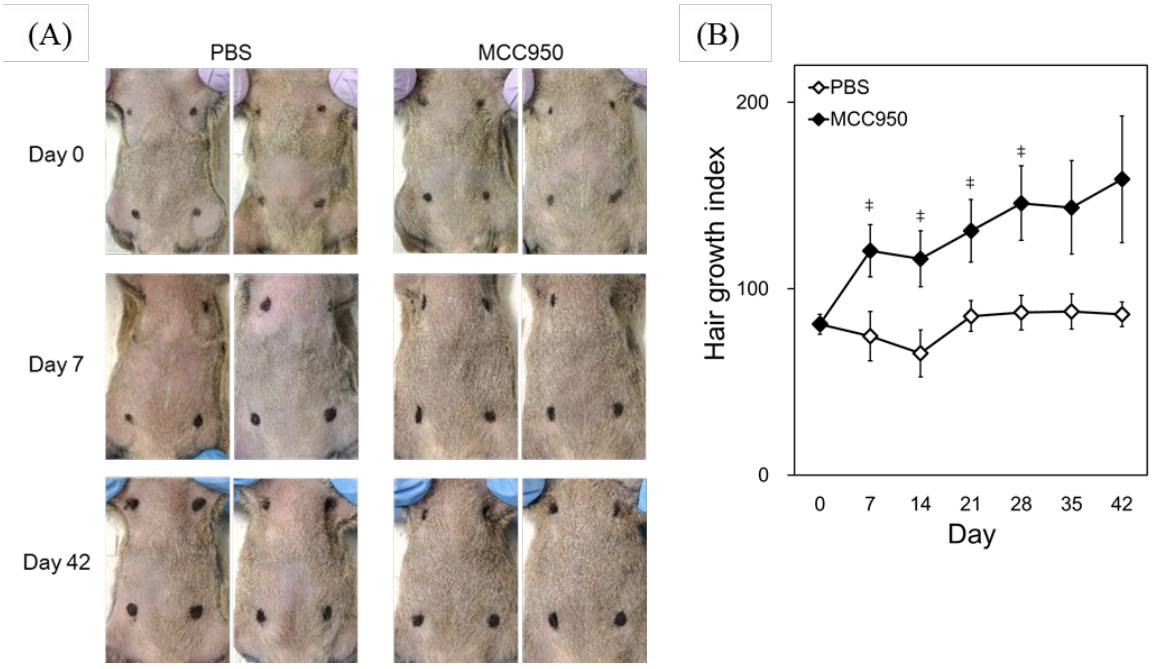

Fig. 3-3. Effect of MCC950 on hair growth in AA mouse model

AA mice were intraperitoneally injected with MCC950 (20 mg/kg) or PBS on days 0, 1, 3, 6, 8, 10, 13, 15, 17, 20, 22, 24, 27, 29, 31, 34, 36, 38, and 41. (A) Representative abdominal skin of AA mice before (day 0) and after administration (days 7 and 42). (B) Hair growth was evaluated every week. Data are expressed as mean ± SE (N = 5). ‡$p < 0.05$. (Student's *t*-test)

(A)

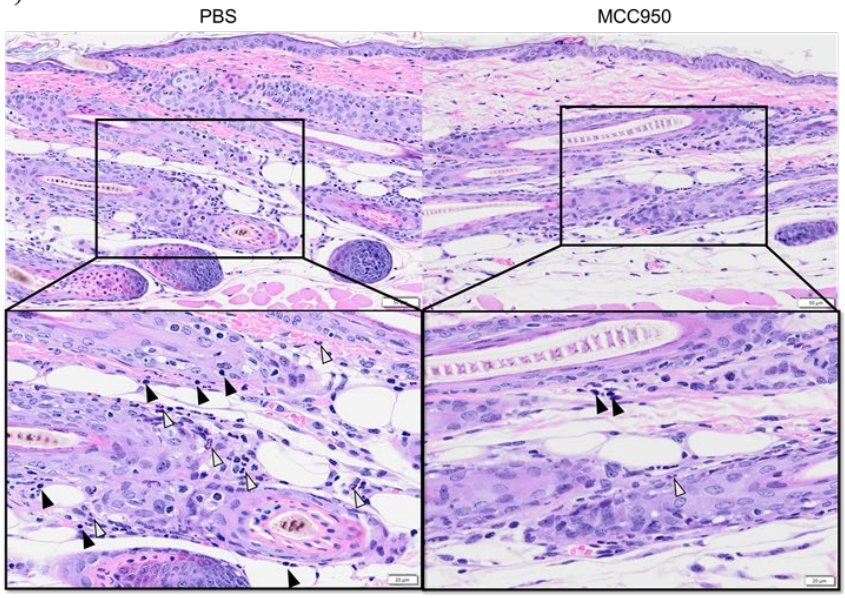
PBS
MCC950

(B)

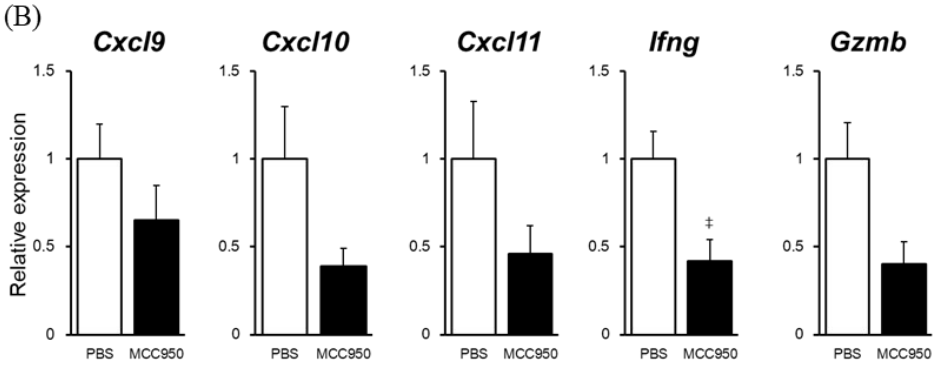
Cxcl9
Cxcl10
Cxcl11
Ifng
Gzmb
Relative expression
1.5
1
0.5
0
PBS
MCC950
‡

(C)

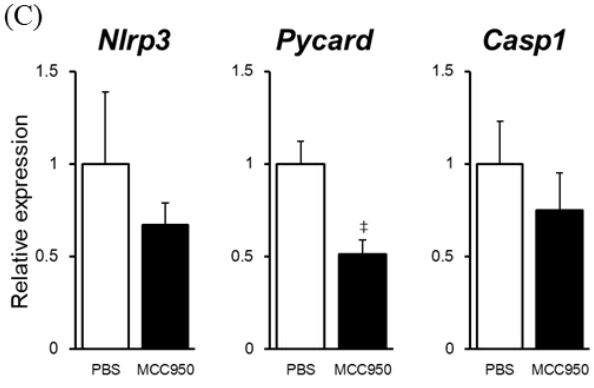
Nlrp3
Pycard
Casp1
Relative expression
1.5
1
0.5
0
PBS
MCC950
‡

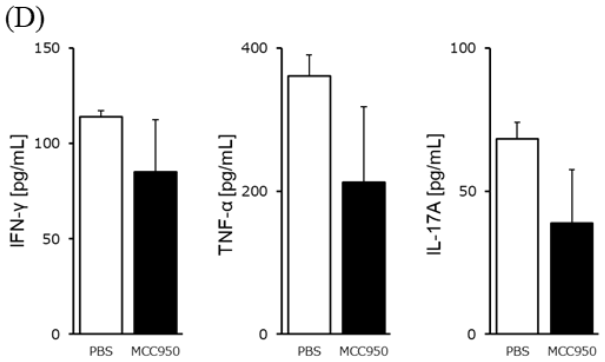

Fig. 3-4. Effect of MCC950 on immune pathophysiological changes in AA mouse model

AA mice were intraperitoneally injected with MCC950 (20 mg/kg) or PBS on days 0, 1, 3, and 6. (A) H&E staining of the skin from PBS- and MCC950-treated mice on day 7. Neutrophils and lymphocytes are marked with white and black arrows, respectively. (B, C) mRNA expressions of CXCL9/10/11, IFN-γ, granzyme B, NLRP3, ASC, and caspase-1 in skin were assessed by RT-qPCR, and the expression levels are shown relative to PBS-treated mice. (D) IFN-γ, TNF-α, and IL-17A levels in serum were measured by multiplex. Data are expressed as mean ± SE (N = 3). ‡$p < 0.05$. (Student's *t*-test).

3.4 Discussion

AA is thought to arise as a consequence of the collapse of local IP with cytotoxicity induced by $CD8^+$ T cells and NK cells (18). Although several studies imply that AA results primarily from dysregulation of innate immunity, similar to other autoimmune diseases (17), the trigger of IP collapse has not been clarified. Here, we compared serum and skin levels of innate immune-related factors between naïve mice, unaffected mice, and AA-affected mice (acute phase and chronic phase). This is the first study to demonstrate that NLRP3 inflammasome activation contributes to development and aggravation of AA and that NLRP3 inhibition may have potential for AA therapy.

In this study, we focused on IFN-α-producing pDCs and NLRP3 inflammasome in innate immunity, and investigated their contributions to AA onset using a C3H/HeJ AA mouse model, which is the most popular and well-defined model for AA. First, we found that IFN-α in serum was upregulated in unaffected mice, whereas its expression in skin was unchanged (Fig. 3-1A, B). Skin IFN-α level was upregulated in lesions of the acute-AA and chronic-AA mice (Fig. 3-1B). Our data demonstrate that IFN-α (all subtypes) protein level was higher in lesions than in non-lesional areas, whereas a previous report showed that IFN-α2 and IFN-α4 mRNA expression was higher in non-lesional areas than in lesions (61). This discrepancy could be caused by differences of IFN-α subtype, definition of non-lesions (normal hairy areas remote from lesions in this study; the vicinity of lesions in the previous report), AA mouse model (induced by cell-transferring or spontaneously affected), and immune status due to aging (our AA-affected mice were younger than 32 weeks old, but the mice in the previous report were 1 year old). IFN-α production is activated by TLR7/9 signaling that requires the formation of a complex consisting of MyD88 (myeloid differentiation factor 88), TRAF3/6, IRAK1/4, and IRF7 (86-88). We found that these adaptor molecules and transcriptional factors were also highly expressed in skin of AA-affected mice, particularly in lesions of the acute-AA mice (Fig. 3-1C–E). These data indicate that the IFN-α signal pathway is locally activated in non-lesional areas in the acute phase. A number of studies have suggested the relevance of TLRs to autoimmune diseases and to triggering IFN-α production. HMGB1-DNA immune complex activates TLR9 and induces pDC activation followed by IFN-α

secretion (84). HMGB1 is released from pDCs after stimulation and regulates IFN-α production via RAGE in an autocrine way (89). HMGB1 is also shown to be released from damaged cells, based on *in vitro* study indicating that outer root sheath cells, which are non-professional immune cells, secrete HMGB1 by poly(I:C)-mediated TLR3 activation (81). In AA patients, HMGB1 levels in scalp and serum have been reported to be upregulated, compared with normal controls (90). HSP70 has also been reported to induce pDC activation and IFN-α production (85). Moreover, the previous study for investigating the effect of heat treatment on AA development has suggested that induction of HSP70 may precipitate the development of AA in C3H/HeJ mice (91). We investigated whether these factors activate pDCs, and showed that mRNA expressions of HMGB1, RAGE, and HSP70 were increased in lesions in the acute phase (Fig. 3-1F–H). Serum level of HSP70 was also increased in the acute phase (Fig. 3-1I). These results indicate that these factors might induce IFN-α production in lesions in the acute phase of AA.

Although NLRP3 inflammasome has been reported to be associated with AA pathogenesis, little is known about its role in AA onset. Our data showed that IL-1β level was increased in both serum and skin before and after AA onset (Fig. 3-2A, E), whereas IFN-α level was increased in lesions after AA onset (Fig. 3-1B). Thus, the increase of IL-1β preceded that of IFN-α, which suggests that increase of IL-1β production results in initiation of innate immune response around immune-privileged HF. IL-18 production is also known to be regulated by NLRP3 inflammasome as well as IL-1β production. Our data showed that IL-18 production was increased in both lesions and non-lesional areas of AA mice (Fig. 3-2F). IL-18 has been reported to induce Th1 and NK cell activation, IFN-γ production (92), and type 1 chemokines (93). The blood level of *mmu-miR-150-5p*, which downregulates IL-18 expression, was lower before and after AA onset than in naïve mice (Fig. 3-2D), which is in concordance with the clinical report that the blood level of *hsa-miR-150-5p* was decreased in AA patients (94). These data support the involvement of IL-18 secretion in AA pathogenesis. The expressions of NLRP3 inflammasome components (NLRP3, ASC, and caspase-1) were highly increased in lesions in the acute phase and also upregulated in non-lesional areas and lesions in the chronic phase (Fig. 3-2H–J). The increase of these factors in skin of AA-affected mice is in agreement with

clinical observations showing that NLRP3, ASC, and caspase-1 were significantly increased in the outer root sheath of HF in AA scalp skin (81). IFN-γ is revealed to play a crucial role in the pathogenesis of AA and their levels in serum and skin tended to increase in mice injected with LN cells compared to naïve mice (Fig. 3-2C, G). It is still unclear if IFN-γ induces NLRP3 inflammasome or NLRP3 activation induces IFN-γ secretion in this study. Whereas the level of IFN-γ in skin was unchanged among pre-AA, acute-AA and chronic-AA, IL-1β and IL-18 protein levels in skin increased in the acute and chronic phases compared with pre-onset (unaffected). Contribution of IL-1β and IL-18 to exacerbation of AA might be larger than that of IFN-γ. Taken together, our data suggest that activation of NLRP3 inflammasome contributes to exacerbation as well as development of AA.

MCC950 is a potent, selective small molecule inhibitor of NLRP3, and its therapeutic effects on various autoimmune diseases have recently been anticipated (95). In the AA mouse model, MCC950 treatment prevented AA development and promoted hair growth (Fig. 3-3A, B). The effect of MCC950 was observed just 7 days after first administration, and we investigated pathological characteristics on day 7. H&E staining revealed that MCC950 treatment reduced infiltration of inflammatory cells such as neutrophils and lymphocytes (Fig. 3-4A). The treatment also reduced expressions of type 1 chemokines, type 1 cytokine, and cytotoxic marker, which were increased in AA-affected mice, as well as NLRP3 inflammasome-related factors (Fig. 3-4B, C). Serum levels of IFN-γ, TNF-α, and IL-17A, which were increased in both AA patients and mice (data not shown), were decreased following MCC950 treatment (Fig. 3-4D). IL-1β is shown to inhibit hair elongation in HF culture (96). IL-18 induces IFN-γ production and, vice versa, IFN-γ induces IL-1β and IL-18 production via NLRP3 inflammasome activation (97, 98). We speculate that MCC950 inhibits the negative loop of IFN-γ and NLRP3 inflammasome and reduces Th1/Tc1 activation, consequently exerting a hair growth effect in AA mice. This study sheds light on pharmacotherapy targeting the innate immune systems for AA, unlike the conventional pharmacological strategy which targets T cells. Considering these findings that NLRP3 inflammasome activation contributes to not only AA exacerbation but also AA initiation, MCC950 might have not only

therapeutic effect but also preventive effect on AA relapse. Further studies will be needed to address whether NLRP3 inhibitor has a preventive effect against AA.

In conclusion, we reported that the IFN-α-producing pathway was activated in lesions in the acute phase, whereas the NLRP3 inflammasome pathway was activated before as well as after AA onset. Furthermore, administration of NLRP3 inflammasome inhibitor MCC950 induced hair regrowth and inhibited infiltration of inflammatory cells, expression of type 1 chemokines and cytokine in skin, and inflammatory cytokines in serum. The inhibitors of NLRP3 inflammasome may be candidates for novel therapeutic agents for AA.

Summary and Conclusion

Chapter 1

This study clarified that T cell subpopulations contributing to pathogenesis of AA are different between the acute and chronic phases, based on the results: $CD4^+$ T_{EM} cells increased in SDLNs before AA onset; $CD8^+$ memory T cells systemically increased in the acute phase; $CD8^+$ T_{CM} cells remained in circulation and $CD8^+$ T_{EM} cells migrated and resided in the local sites, such as SDLNs and skin, in the chronic phase. This study also revealed that the expressions of cytokines, chemokines and antigen presentation-related molecules differ between the disease phases. Moreover, similar to patients with AA, melanogenesis-related proteins, particularly tyrosinase, were directly identified as potential autoreactive targets in AA mouse model.

Chapter 2

The author has established a new method for generating AA mice using cryopreserved lymphocytes, which solves a troublesome matter of requiring not only spontaneously AA-affected mice but also the continuous breeding of AA mice as donor mice. This new method allows the generation of large numbers of AA mice with a high frequency as needed. The pathological characteristics of AA mice generated with the new method were similar to those of AA patients including inflammatory cell infiltration around anagen HFs and the upregulated expressions of cytokines and chemokines. These findings also suggest that T_{EM} cells and $CD11c^+$ DCs contribute to the induction of AA. This convenient and reproducible method is expected to be valuable for AA study.

Chapter 3

This study demonstrated that innate immune systems, such as IFN-α-producing pDCs and NLRP3 inflammasome, contribute to the pathogenesis of AA. In particular, this study clarified that activation of NLRP3 inflammasome contributes to both AA initiation and exacerbation by comparing before and after AA onset. Moreover, the treatment of MCC950, a selective NLRP3 inhibitor, prevented AA development and promoted hair growth by reducing NLRP3 signaling and Th1/Tc1 immune responses. These findings suggest that the inhibitors of NLRP3 inflammasome may be candidates for novel therapeutic agent for AA.

Conclusion

Through the analysis of the mouse model reflecting AA pathological conditions, this study reveals the difference of the pathology and potential therapeutic targets between the different phages in AA. This study also highlights the importance of innate immunity as well as acquired immunity. These findings could potentially lead to a better understanding of AA pathomechanisms in humans and the development of novel potential therapeutics of AA.

Acknowledgements

The author would like to express her sincere gratitude to Dr. Fumito Tani, Professor of Graduate School of Agriculture, Kyoto University, for his valuable guidance.

The author would like to be grateful to Dr. Tatsumi Matsumoto, Ms. Sachi Mori and Dr. Yoshihito Yamada, Kyoto R&D Center, Maruho Co., Ltd., for their supports including useful advices, helpful discussions, and warm encouragements.

The author would like to thank my colleagues, Mr. Kota Sekiguchi, Dr. Shoichi Matsuda, Ms. Mika Fujikawa, Ms. Narumi Koreto, Mr. Yusuke Kumagai, Ms. Sanae Hirota, Research Department, Kyoto R&D Center, Maruho Co., Ltd., for their experimental technical assistance.

References

1. Mirzoyev SA, Schrum AG, Davis MDP, and Torgerson RR. Lifetime incidence risk of alopecia areata estimated at 2.1% by Rochester Epidemiology Project, 1990-2009. *J. Invest. Dermatol.* 2014;**134**(4):1141-2.
2. Harries M, Macbeth AE, Holmes S, Chiu WS, Gallardo WR, Nijher M, et al. The epidemiology of alopecia areata: a population-based cohort study in UK primary care. *Br. J. Dermatol.* 2022;**186**(2):257-65.
3. Tan E, Tay YK, Goh CL, and Chin Giam Y. The pattern and profile of alopecia areata in Singapore--a study of 219 Asians. *Int. J. Dermatol.* 2002;**41**(11):748-53.
4. Rencz F, Gulácsi L, Péntek M, Wikonkál N, Baji P, and Brodszky V. Alopecia areata and health-related quality of life: a systematic review and meta-analysis. *Br. J. Dermatol.* 2016;**175**(3):561-71.
5. Liu LY, King BA, and Craiglow BG. Health-related quality of life (HRQoL) among patients with alopecia areata (AA): A systematic review. *J. Am. Acad. Dermatol.* 2016;**75**(4):806-12.
6. Cranwell WC, Lai VW, Photiou L, Meah N, Wall D, Rathnayake D, et al. Treatment of alopecia areata: An Australian expert consensus statement. *Australas. J. Dermatol.* 2019;**60**(2):163-70.
7. Pericin M, and Trüeb RM. Topical immunotherapy of severe alopecia areata with diphenylcyclopropenone: evaluation of 68 cases. *Dermatology* 1998;**196**(4):418-21.
8. Manimaran RP, Ramassamy S, Rajappa M, and Chandrashekar L. Therapeutic outcome of diphencyprone and its correlation with serum cytokine profile in alopecia areata. *J. Dermatolog. Treat.* 2022;**33**(1):324-8.
9. Liu LY, Craiglow BG, Dai F, and King BA. Tofacitinib for the treatment of severe alopecia areata and variants: A study of 90 patients. *J. Am. Acad. Dermatol.* 2017;**76**(1):22-8.
10. Nakajima T, Inui S, and Itami S. Pulse corticosteroid therapy for alopecia areata: study of 139 patients. *Dermatology* 2007;**215**(4):320-4.

11. Nowaczyk J, Makowska K, Rakowska A, Sikora M, and Rudnicka L. Cyclosporine with and without systemic corticosteroids in treatment of alopecia areata: A Systematic Review. *Dermatol. Ther. (Heidelb).* 2020;**10**(3):387-99.
12. Trüeb RM, and Dias M. Alopecia areata: a comprehensive review of pathogenesis and management. *Clin. Rev. Allergy. Immunol.* 2018;**54**(1):68-87.
13. Lee S, and Lee WS. Management of alopecia areata: Updates and algorithmic approach. *J. Dermatol.* 2017;**44**(11):1199-211.
14. Meah N, Wall D, York K, Bhoyrul B, Bokhari L, Sigall DA, et al. The Alopecia Areata Consensus of Experts (ACE) study: Results of an international expert opinion on treatments for alopecia areata. *J. Am. Acad. Dermatol.* 2020;**83**(1):123-30.
15. Fukuyama M, Ito T, and Ohyama M. Alopecia areata: Current understanding of the pathophysiology and update on therapeutic approaches, featuring the Japanese Dermatological Association guidelines. *J. Dermatol.* 2022;**49**(1):19-36.
16. Darwin E, Hirt PA, Fertig R, Doliner B, Delcanto G, Jimenez JJ. Alopecia areata: Review of epidemiology, clinical features, pathogenesis, and new treatment options. *Int. J. Trichol*. 2018;**10**:51-60.
17. Rajabi F, Drake LA, Senna MM, and Rezaei N. Alopecia areata: a review of disease pathogenesis. *Br. J. Dermatol.* 2018;**179**(5):1033-48.
18. Bertolini M, McElwee K, Gilhar A, Bulfone-Paus S, and Paus R. Hair follicle immune privilege and its collapse in alopecia areata. *Exp. Dermatol.* 2020;**29**(8):703-25.
19. Pratt CH, King LE, Jr., Messenger AG, Christiano AM, and Sundberg JP. Alopecia areata. *Nat. Rev. Dis. Primers.* 2017;**3**:17011.
20. Strazzulla LC, Wang EHC, Avila L, Lo Sicco K, Brinster N, Christiano AM, et al. Alopecia areata: Disease characteristics, clinical evaluation, and new perspectives on pathogenesis. *J. Am. Acad. Dermatol.* 2018;**78**(1):1-12.
21. Petukhova L, Duvic M, Hordinsky M, Norris D, Price V, Shimomura Y, et al. Genome-wide association study in alopecia areata implicates both innate and adaptive immunity. *Nature* 2010;**466**(7302):113-7.

22. de Jong A, Jabbari A, Dai Z, Xing L, Lee D, Li MM, et al. High-throughput T cell receptor sequencing identifies clonally expanded CD8+ T cell populations in alopecia areata. *JCI Insight* 2018;**3**(19):e121949.
23. Wang EHC, Yu M, Breitkopf T, Akhoundsadegh N, Wang X, Shi FT, et al. Identification of autoantigen epitopes in Alopecia Areata. *J. Invest. Dermatol.* 2016;**136**(8):1617-26.
24. Leung MC, Sutton CW, Fenton DA, and Tobin DJ. Trichohyalin is a potential major autoantigen in human alopecia areata. *J. Proteome. Res.* 2010;**9**(10):5153-63.
25. Erb U, Freyschmidt-Paul P, and Zöller M. Tolerance induction by hair-specific keratins in murine alopecia areata. *J. Leukoc. Biol.* 2013;**94**(4):845-57.
26. Ito T, Bertolini M, Funakoshi A, Ito N, Takayama T, Biro T, et al. Presence of MAGE-A3 specific T cells in alopecia areata - study for the possibility of AA antigens -. *J. Dermatol. Sci.* 2013;**72**:327-30.
27. Gilhar A, Schrum AG, Etzioni A, Waldmann H, and Paus R. Alopecia areata: Animal models illuminate autoimmune pathogenesis and novel immunotherapeutic strategies. *Autoimmun. Rev.* 2016;**15**(7):726-35.
28. Sundberg JP, McElwee K, Brehm MA, Su L, and King LE, Jr. Animal models for alopecia areata: What and Where? *J. Investig. Dermatol. Symp. Proc.* 2015;**17**(2):23-6.
29. Sun J, Silva KA, McElwee KJ, King LE, Jr., and Sundberg JP. The C3H/HeJ mouse and DEBR rat models for alopecia areata: review of preclinical drug screening approaches and results. *Exp. Dermatol.* 2008;**17**(10):793-805.
30. Sundberg JP, Cordy WR, and King LE, Jr. Alopecia areata in aging C3H/HeJ mice. *J. Invest. Dermatol.* 1994;**102**(6):847-56.
31. Wang EHC, Khosravi-Maharlooei M, Jalili RB, Yu R, Ghahary A, Shapiro J, et al. Transfer of alopecia areata to C3H/HeJ mice using cultured lymph node-derived cells. *J. Invest. Dermatol.* 2015;**135**(10):2530-2.

32. Wang EHC, and McElwee KJ. Nonsurgical induction of alopecia areata in C3H/HeJ Mice via adoptive transfer of cultured lymphoid cells. *Methods Mol. Biol.* 2020;**2154**:121-31.
33. Freyschmidt-Paul P, Sundberg JP, Happle R, McElwee KJ, Metz S, Boggess D, et al. Successful treatment of alopecia areata-like hair loss with the contact sensitizer squaric acid dibutylester (SADBE) in C3H/HeJ mice. *J. Invest. Dermatol.* 1999;**113**(1):61-8.
34. Xing L, Dai Z, Jabbari A, Cerise JE, Higgins CA, Gong W, et al. Alopecia areata is driven by cytotoxic T lymphocytes and is reversed by JAK inhibition. *Nat. Med.* 2014;**20**(9):1043-9.
35. Friedli A, Labarthe MP, Engelhardt E, Feldmann R, Salomon D, and Saurat JH. Pulse methylprednisolone therapy for severe alopecia areata: an open prospective study of 45 patients. *J. Am. Acad. Dermatol.* 1998;**39**(4 Pt 1):597-602.
36. Paus R, Slominski A, and Czarnetzki BM. Is alopecia areata an autoimmune-response against melanogenesis-related proteins, exposed by abnormal MHC class I expression in the anagen hair bulb? *Yale. J. Biol. Med.* 1993;**66**(6):541-54.
37. Tilney NL. Patterns of lymphatic drainage in the adult laboratory rat. *J. Anat.* 1971;**109**(Pt 3):369-83.
38. Suárez-Fariñas M, Ungar B, Noda S, Shroff A, Mansouri Y, Fuentes-Duculan J, et al. Alopecia areata profiling shows TH1, TH2, and IL-23 cytokine activation without parallel TH17/TH22 skewing. *J. Allergy Clin. Immunol.* 2015;**136**(5):1277-87.
39. Perret C, Wiesner-Menzel L, and Happle R. Immunohistochemical analysis of T-cell subsets in the peribulbar and intrabulbar infiltrates of alopecia areata. *Acta. Derm. Venereol.* 1984;**64**(1):26-30.
40. Ito T, Ito N, Saatoff M, Hashizume H, Fukamizu H, Nickoloff BJ, et al. Maintenance of hair follicle immune privilege is linked to prevention of NK cell attack. *J. Invest. Dermatol.* 2008;**128**(5):1196-206.
41. Ito T, Hashizume H, Shimauchi T, Funakoshi A, Ito N, Fukamizu H, et al. CXCL10 produced from hair follicles induces Th1 and Tc1 cell infiltration in the

acute phase of alopecia areata followed by sustained Tc1 accumulation in the chronic phase. *J. Dermatol. Sci.* 2013;**69**(2):140-7.

42. Agamia N, Apalla Z, El Achy S, Abdelmaksoud E, Kandil N, and Abozeid S. Interferon-gamma serum level and immunohistochemical expression of CD8 cells in tissue biopsies in patients with alopecia areata in correlation with trichoscopic findings. *Dermatol. Ther.* 2020;**33**(4):e13718.
43. Dai Z, Xing L, Cerise J, Wang EH, Jabbari A, de Jong A, et al. CXCR3 blockade inhibits T cell migration into the skin and prevents development of alopecia areata. *J. Immunol.* 2016;**197**(4):1089-99.
44. Farber DL, Yudanin NA, and Restifo NP. Human memory T cells: generation, compartmentalization and homeostasis. *Nat. Rev. Immunol.* 2014;**14**(1):24-35.
45. Ho AW, and Kupper TS. T cells and the skin: from protective immunity to inflammatory skin disorders. *Nat. Rev. Immunol.* 2019;**19**(8):490-502.
46. Borcherding N, Crotts SB, Ortolan LS, Henderson N, Bormann NL, and Jabbari A. A transcriptomic map of murine and human alopecia areata. *JCI Insight* 2020;**5**(13):e137424.
47. Subramanya RD, Coda AB, and Sinha AA. Transcriptional profiling in alopecia areata defines immune and cell cycle control related genes within disease-specific signatures. *Genomics* 2010;**96**(3):146-53.
48. Förster R, Davalos-Misslitz AC, and Rot A. CCR7 and its ligands: balancing immunity and tolerance. *Nat. Rev. Immunol.* 2008;**8**(5):362-71.
49. Gately MK, Gubler U, Brunda MJ, Nadeau RR, Anderson TD, Lipman JM, et al. Interleukin-12: a cytokine with therapeutic potential in oncology and infectious diseases. *Ther. Immunol.* 1994;**1**(3):187-96.
50. Liu T, Li S, Ying S, Tang S, Ding Y, Li Y, et al. The IL-23/IL-17 Pathway in Inflammatory Skin Diseases: From Bench to Bedside. *Front. Immunol.* 2020;**11**:594735.
51. Rittié L, and Elder JT. Capturing the finer points of gene expression in psoriasis: Beaming in on the CCL19/CCR7 axis. *J. Invest. Dermatol.* 2012;**132**(6):1535-8.

52. Ito T, Ito N, Bettermann A, Tokura Y, Takigawa M, and Paus R. Collapse and restoration of MHC class-I-dependent immune privilege: exploiting the human hair follicle as a model. *Am. J. Pathol.* 2004;**164**(2):623-34.
53. Bröcker EB, Echternacht-Happle K, Hamm H, and Happle R. Abnormal expression of class I and class II major histocompatibility antigens in alopecia areata: modulation by topical immunotherapy. *J. Invest. Dermatol.* 1987;**88**(5):564-8.
54. Kemp EH, Sandhu HK, Weetman AP, and McDonagh AJ. Demonstration of autoantibodies against tyrosine hydroxylase in patients with alopecia areata. *Br. J. Dermatol.* 2011;**165**(6):1236-43.
55. McElwee KJ, Boggess D, King LE, Jr., and Sundberg JP. Experimental induction of alopecia areata-like hair loss in C3H/HeJ mice using full-thickness skin grafts. *J. Invest. Dermatol.* 1998;**111**(5):797-803.
56. Olsen E, Hordinsky M, McDonald-Hull S, Price V, Roberts J, Shapiro J, et al. Alopecia areata investigational assessment guidelines. National Alopecia Areata Foundation. *J. Am. Acad. Dermatol.* 1999;**40**(2 Pt 1):242-6.
57. Zhang X, Zhao Y, Ye Y, Li S, Qi S, Yang Y, et al. Lesional infiltration of mast cells, Langerhans cells, T cells and local cytokine profiles in alopecia areata. *Arch. Dermatol. Res.* 2015;**307**(4):319-31.
58. Nakamura M, Jo J, Tabata Y, and Ishikawa O. Controlled delivery of T-box21 small interfering RNA ameliorates autoimmune alopecia (Alopecia Areata) in a C3H/HeJ mouse model. *Am. J. Pathol.* 2008;**172**(3):650-8.
59. Elela MA, Gawdat HI, Hegazy RA, Fawzy MM, Abdel Hay RM, Saadi D, et al. B cell activating factor and T-helper 17 cells: possible synergistic culprits in the pathogenesis of Alopecia Areata. *Arch. Dermatol. Res.* 2016;**308**(2):115-21.
60. Tanemura A, Oiso N, Nakano M, Itoi S, Kawada A, and Katayama I. Alopecia areata: infiltration of Th17 cells in the dermis, particularly around hair follicles. *Dermatology* 2013;**226**(4):333-6.

61. Ito T, Suzuki T, Sakabe JI, Funakoshi A, Fujiyama T, and Tokura Y. Plasmacytoid dendritic cells as a possible key player to initiate alopecia areata in the C3H/HeJ mouse. *Allergol. Int.* 2020;**69**(1):121-31.

62. Abou Rahal J, Kurban M, Kibbi AG, and Abbas O. Plasmacytoid dendritic cells in alopecia areata: missing link? *J. Eur. Acad. Dermatol. Venereol.* 2016;**30**(1):119-23.

63. Gao Z, Jin YQ, and Wu W. SOCS3 treatment prevents the development of alopecia areata by inhibiting $CD8^+$ T cell-mediated autoimmune destruction. *Oncotarget.* 2017;**8**(20):33432-43.

64. McElwee KJ, Freyschmidt-Paul P, Hoffmann R, Kissling S, Hummel S, Vitacolonna M, et al. Transfer of $CD8^+$ cells induces localized hair loss whereas $CD4^+/CD25^-$ cells promote systemic alopecia areata and $CD4^+/CD25^+$ cells blockade disease onset in the C3H/HeJ mouse model. *J. Invest. Dermatol.* 2005;**124**(5):947-57.

65. Skinner RB, Jr., Light WH, Bale GF, Rosenberg EW, and Leonardi C. Alopecia areata and presence of cytomegalovirus DNA. *JAMA.* 1995;**273**(18):1419-20.

66. Ito T, and Tokura Y. Alopecia areata triggered or exacerbated by swine flu virus infection. *J. Dermatol.* 2012;**39**(10):863-4.

67. Kartal ED, Alpat SN, Ozgunes I, and Usluer G. Reversible alopecia universalis secondary to PEG-interferon alpha-2b and ribavirin combination therapy in a patient with chronic hepatitis C virus infection. *Eur. J. Gastroenterol. Hepatol.* 2007;**19**(9):817-20.

68. Azzawi S, Penzi LR, and Senna MM. Immune privilege collapse and alopecia development: Is stress a factor. *Skin Appendage Disord.* 2018;**4**(4):236-44.

69. Acharya P, and Mathur MC. Oxidative stress in alopecia areata: a systematic review and meta-analysis. *Int. J. Dermatol.* 2020;**59**(4):434-40.

70. Kawai T, and Akira S. The role of pattern-recognition receptors in innate immunity: update on Toll-like receptors. *Nat. Immunol.* 2010;**11**(5):373-84.

71. Li Z, Guo J, and Bi L. Role of the NLRP3 inflammasome in autoimmune diseases. *Biomed. Pharmacother.* 2020;**130**:110542.

72. Wu YW, Tang W, and Zuo JP. Toll-like receptors: potential targets for lupus treatment. *Acta Pharmacol. Sin.* 2015;**36**(12):1395-407.
73. Arleevskaya MI, Larionova RV, Brooks WH, Bettacchioli E, and Renaudineau Y. Toll-like receptors, infections, and rheumatoid arthritis. *Clin. Rev. Allergy Immunol.* 2020;**58**(2):172-81.
74. Yehualashet AS. Toll-like receptors as a potential drug target for diabetes mellitus and diabetes-associated complications. *Diabetes Metab. Syndr. Obes.* 2020;**13**:4763-77.
75. Sun L, Liu W, and Zhang LJ. The role of Toll-like receptors in skin host defense, psoriasis, and atopic dermatitis. *J. Immunol. Res.* 2019;**2019**:1824624.
76. Frasca L, and Lande R. Toll-like receptors in mediating pathogenesis in systemic sclerosis. *Clin. Exp. Immunol.* 2020;**201**(1):14-24.
77. Alzolibani AA, Rasheed Z, Bin Saif G, Al-Dhubaibi MS, and Al Robaee AA. Altered expression of intracellular Toll-like receptors in peripheral blood mononuclear cells from patients with alopecia areata. *BBA Clin.* 2016;**5**:134-42.
78. Kang H, Wu WY, Yu M, Shapiro J, and McElwee KJ. Increased expression of TLR7 and TLR9 in alopecia areata. *Exp. Dermatol.* 2020;**29**(3):254-8.
79. Ghoreishi M, Martinka M, and Dutz JP. Type 1 interferon signature in the scalp lesions of alopecia areata. *Br. J. Dermatol.* 2010;**163**(1):57-62.
80. Little AJ, and Vesely MD. Cutaneous lupus erythematosus: Current and future pathogenesis-directed therapies. *Yale. J. Biol. Med.* 2020;**93**(1):81-95.
81. Shin JM, Choi DK, Sohn KC, Kim SY, Min Ha J, Ho Lee Y, et al. Double-stranded RNA induces inflammation via the NF-κB pathway and inflammasome activation in the outer root sheath cells of hair follicles. *Sci. Rep.* 2017;**7**:44127.
82. Lee D, Hong SK, Park SW, Hur DY, Shon JH, Shin JG, et al. Serum levels of IL-18 and sIL-2R in patients with alopecia areata receiving combined therapy with oral cyclosporine and steroids. *Exp. Dermatol.* 2010;**19**(2):145-7.
83. Kim SK, Park HJ, Chung JH, Kim JW, Seok H, Lew BL, et al. Association between interleukin 18 polymorphisms and alopecia areata in Koreans. *J. Interferon Cytokine Res.* 2014;**34**(5):349-53.

84. Tian J, Avalos AM, Mao SY, Chen B, Senthil K, Wu H, et al. Toll-like receptor 9-dependent activation by DNA-containing immune complexes is mediated by HMGB1 and RAGE. *Nat. Immunol.* 2007;**8**(5):487-96.

85. Jacquemin C, Rambert J, Guillet S, Thiolat D, Boukhedouni N, Doutre MS, et al. Heat shock protein 70 potentiates interferon alpha production by plasmacytoid dendritic cells: relevance for cutaneous lupus and vitiligo pathogenesis. *Br. J. Dermatol.* 2017;**177**(5):1367-75.

86. Kawai T, Sato S, Ishii KJ, Coban C, Hemmi H, Yamamoto M, et al. Interferon-alpha induction through Toll-like receptors involves a direct interaction of IRF7 with MyD88 and TRAF6. *Nat. Immunol.* 2004;**5**(10):1061-8.

87. Oganesyan G, Saha SK, Guo B, He JQ, Shahangian A, Zarnegar B, et al. Critical role of TRAF3 in the Toll-like receptor-dependent and -independent antiviral response. *Nature* 2006;**439**(7073):208-11.

88. Honda K, Yanai H, Mizutani T, Negishi H, Shimada N, Suzuki N, et al. Role of a transductional-transcriptional processor complex involving MyD88 and IRF-7 in Toll-like receptor signaling. *Proc. Natl. Acad. Sci. U S A.* 2004;**101**(43):15416-21.

89. Dumitriu IE, Baruah P, Bianchi ME, Manfredi AA, and Rovere-Querini P. Requirement of HMGB1 and RAGE for the maturation of human plasmacytoid dendritic cells. *Eur. J. Immunol.* 2005;**35**(7):2184-90.

90. Lee Y, Lee HE, Shin JM, Sohn KC, Im M, Kim CD, et al. Clinical significance of serum high-mobility group box 1 level in alopecia areata. *J. Am. Acad. Dermatol.* 2013;**69**(5):742-7.

91. Wikramanayake TC, Alvarez-Connelly E, Simon J, Mauro LM, Guzman J, Elgart G, et al. Heat treatment increases the incidence of alopecia areata in the C3H/HeJ mouse model. *Cell Stress Chaperones* 2010;**15**(6):985-91.

92. Kaplanski G. Interleukin-18: Biological properties and role in disease pathogenesis. *Immunol. Rev.* 2018;**281**(1):138-53.

93. Kanda N, Shimizu T, Tada Y, and Watanabe S. IL-18 enhances IFN-gamma-induced production of CXCL9, CXCL10, and CXCL11 in human keratinocytes. *Eur. J. Immunol.* 2007;**37**(2):338-50.

94. Sheng Y, Qi S, Hu R, Zhao J, Rui W, Miao Y, et al. Identification of blood microRNA alterations in patients with severe active alopecia areata. *J. Cell Biochem.* 2019;**120**(9):14421-30.

95. Coll RC, Robertson AA, Chae JJ, Higgins SC, Muñoz-Planillo R, Inserra MC, et al. A small-molecule inhibitor of the NLRP3 inflammasome for the treatment of inflammatory diseases. *Nat. Med.* 2015;**21**(3):248-55.

96. Harmon CS, and Nevins TD. IL-1 alpha inhibits human hair follicle growth and hair fiber production in whole-organ cultures. *Lymphokine Cytokine Res.* 1993;**12**(4):197-203.

97. Shin JM, Choi DK, Sohn KC, Koh JW, Lee YH, Seo YJ, et al. Induction of alopecia areata in C3H/HeJ mice using polyinosinic-polycytidylic acid (poly[I:C]) and interferon-gamma. *Sci. Rep.* 2018;**8**(1):12518.

98. Kim JE, Lee YJ, Park HR, Lee DG, Jeong KH, and Kang H. The effect of JAK inhibitor on the survival, anagen re-entry, and hair follicle immune privilege restoration in human dermal papilla cells. *Int. J. Mol. Sci.* 2020;**21**(14):5137.

Copyright Notice

The contents described in Chapter 1 to Chapter 3 were originally published as follows:

Hashimoto K, et al. Altered T cell subpopulations and serum anti-TYRP2 and tyrosinase antibodies in the acute and chronic phase of alopecia areata in the C3H/HeJ mouse model. *J. Dermatol. Sci.* 2021;**104**(1):21-29.
DOI: 10.1016/j.jdermsci.2021.09.001

Hashimoto K, et al. Induction of alopecia areata in C3H/HeJ mice using cryopreserved lymphocytes. *J. Dermatol. Sci.* 2021;**102**(3):177-183.
DOI: 10.1016/j.jdermsci.2021.04.009

Hashimoto K, et al. NLRP3 inflammasome activation contributes to development of alopecia areata in C3H/HeJ mice. *Exp. Dermatol.* 2022;**31**(2):133-142.
DOI: 10.1111/exd.14432

Fig. G-1 and Fig. G-3 were originally published as follows:
Darwin E, et al. Alopecia areata: Review of epidemiology, clinical features, pathogenesis, and new treatment options. *Int. J. Trichol.* 2018;**10**:51-60.
DOI: 10.4103/ijt.ijt_99_17